Advances in Water Resources 140 (2020) 103565

Contents lists available at ScienceDirect

Advances in Water Resources

journal homepage: www.elsevier.com/locate/advwatres

# Predicting transport characteristics of hyperuniform porous media via rigorous microstructure-property relations

Salvatore Torquato*

*Department of Chemistry, Department of Physics, Princeton Institute for the Science and Technology of Materials, and Program in Applied and Computational Mathematics, Princeton University, Princeton, New Jersey 08544, USA*

A B S T R A C T

This paper is concerned with the estimation of the effective transport characteristics of fluid-saturated porous media via rigorous microstructure-property relations. We are particularly interested in predicting the formation factor $\mathcal{F}$, mean survival time $\tau$, principal NMR (diffusion) relaxation time $T_1$, principal viscous relaxation time $\Theta_1$, and fluid permeability $k$. To do so, we employ rigorous methods to estimate the fluid permeability and these other transport properties of "hyperuniform" and nonhyperuniform models of porous media from microstructural information. Disordered hyperuniform materials are exotic amorphous states of matter that have attracted great attention in the physical, mathematical and biological science but little is known about their fluid transport characteristics. In carrying out this investigation, we not only draw from ideas and results of the emerging field of hyperuniformity, but from homogenization theory, statistical geometry, differential equations (spectrum of Laplace and Stokes operators), and the covering and quantizer problems of discrete geometry. Among other results, we derive a Fourier representation of a classic rigorous upper bound on the fluid permeability that depends on the spectral density to infer how the permeabilities of hyperuniform porous media perform relative to those of nonhyperuniform ones. We find that the velocity fields in nonhyperuniform porous media are generally much more localized over the pore space compared to those in their hyperuniform counterparts, which has implications for their permeabilities. Rigorous bounds on transport properties suggest a new approximate formula for the fluid permeability that provides reasonably accurate permeability predictions of a certain class of hyperuniform and nonhyperuniform porous media. These comparative studies shed new light on the microstructural characteristics that determine the transport properties of general porous media. Our findings also have implications for the design of porous materials with desirable transport properties.

## 1. Introduction

The physical properties of fluid-saturated porous media are fundamentally controlled by the underlying complex microstructures of these heterogeneous media across length scales. Knowledge of their transport properties is of central importance in hydrology, petroleum engineering and reservoir engineering (Todd and Mays, 2004; Øren et al., 2002; Dandekar, 2013). While these physical properties can be ascertained experimentally by retrieving physical samples and testing them in the laboratory, such methods can be tedious and often do not yield insights about the microstructures. This emphasizes the need for sophisticated mathematical and computational tools that are capable of modeling the complex microstructures and their physical properties. Such methods have been developed over the last several decades. This includes homogenization and averaging methods to estimate the effective transport properties (Quintard and Whitaker, 1994a; 1994b; Milton, 2002; Torquato, 2002b; Sahimi, 2003). Moreover, X-ray microtomographic techniques, which provide three-dimensional (3D) digitized images of porous media at the pore scale in a nondestructive manner (Kinney and Nichols, 1992; Coker et al., 1996; Blunt et al., 2013), have been combined with computational reconstruction techniques (Yeong and Torquato, 1998a; 1998b; Jiao et al., 2009; Tahmasebi and Sahimi, 2013; Tahmasebi, 2018) to produce a wide class of realistic microstructures at will. Subsequently, such computer-generated microstructures can be structurally characterized and their physical properties can be estimated via computer simulations (Sahimi, 2003; Wood et al.,; Bijeljic and Blunt, 2006; Blunt et al., 2013; Vasseur and Wadsworth, 2017; Aramideh et al., 2018).

The effective transport, electromagnetic and mechanical properties of porous and other heterogeneous media generally require information about an infinite set of correlation functions (Brown, 1955; Beran, 1965; Milton, 1987; Sen and Torquato, 1989; Torquato, 1997; Milton, 2002; Torquato, 2002a). Since such complete information is almost never available in practice for general microstructures, theoretical estimates of the effective properties are based either on approximate methods (Scheidegger, 1974; Johnson et al., 1986; Thompson et al., 1987; Martys et al., 1994; Milton, 2002; Torquato, 2002a; Sahimi, 2003) or rigorous upper and lower bounds that account for a finite set of correlation functions (Beran, 1965; Milton, 2002; Torquato, 2002a). The bounds tighten as progressively more microstructural information is properly incorporated.

Our focus in this paper is the use of rigorous theoretical methods to estimate the following effective transport properties of fluid-saturated porous media in terms of various $n$-point correlation functions:

* Corresponding author.
*E-mail address:* torquato@princeton.edu

https://doi.org/10.1016/j.advwatres.2020.103565
Received 27 December 2019; Received in revised form 24 February 2020; Accepted 14 March 2020
Available online 19 March 2020

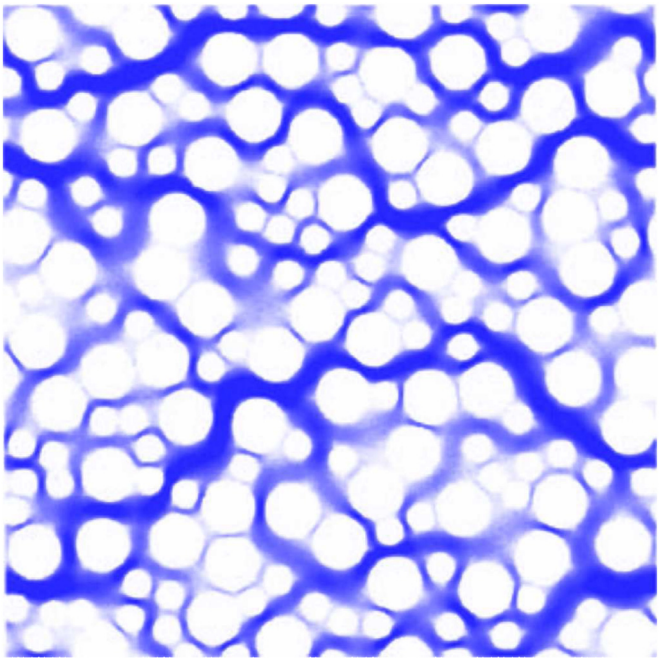

**Fig. 1.** Laminar flow through the void space of a two-dimensional hard-disk packing. The brightness of the color (gray value) indicates the magnitude of the flow velocity. The image is adapted from Ref. Torquato (2002a).

1. Formation factor $F$;
2. Mean survival time $\tau$;
3. Principal NMR (diffusion) relaxation time $T_1$
4. Principal viscous relaxation time $\Theta_1$
5. Fluid permeability $k$

Among these physical properties (which are defined more precisely in Section 3), the most challenging to predict for general microstructures is the fluid permeability $k$, which is defined by Darcy's law. The permeability $k$ has dimensions of the square of length and, roughly speaking, may be regarded as an effective pore channel area of the *dynamically* connected part of the pore space (Torquato, 2002a). By "dynamically" connected, we mean the topologically connected portion of the pore space that carries the flow, which eliminates isolated pores and dead-ends and connected regions with very little flow, for example. Fig. 1 gives visual sense of the dynamically connected pore space for two-dimensional Stokes flow through a bed of nonoverlapping disks. Remarkably, all of the other transport properties in the list above, $F$, $\tau$, $T_1$ and $\Theta_1$, are intimately related to the fluid permeability $k$, as we will discuss and exploit subsequently.

We are particularly interested in hyperuniform porous media. A hyperuniform state of matter is characterized by an anomalous suppression of density or volume-fraction fluctuations at infinitely long wavelengths relative to those in typical disordered systems, such as liquids and structural glasses (Torquato and Stillinger, 2003; Zachary and Torquato, 2009; Torquato, 2018a). Hyperuniform states include all perfect crystals, many quasicrystals, as well as special disordered systems. Disordered hyperuniform materials are exotic amorphous states of matter that are like crystals in the manner in which their large-scale density fluctuations are anomalously suppressed and yet behave like liquids or glasses in that they are statistically isotropic without any Bragg peaks. They have been the subject of fundamental interest across a variety of fields, including physical (Torquato et al., 2008; Batten et al., 2008; Hexner and Levine, 2015; Weijs et al., 2015; Thien et al., 2017; Chen and Torquato, 2018; Ding et al., 2018; Lomba et al., 2018), mathematical (Ghosh and Lebowitz, 2018; Brauchart et al., 2019; Torquato et al., 2019) and biological (Jiao et al., 2014; Mayer et al., 2015) sciences. It is being discovered that disordered hyperuniform materials can have remarkable physical properties, including cellular materials with complete isotropic photonic band gaps (Florescu et al., 2009; Man et al., 2013; Froufe-Pérez et al., 2017), optimal thermal, diffusive and elastic properties (Zhou et al., 2016; Chen and Torquato, 2018; Kim and Torquato, 2019b), dense but transparent materials Leseur et al. (2016), and devices for enhanced directional light extraction (Gorsky et al., 2019).

Little is known about the fluid transport characteristics of disordered hyperuniform porous media. One exception is a recent study that demonstrated that electrical or fluid transport through disordered hyperuniform networks is optimized in the limit that the porosity tends to zero (Torquato and Chen, 2018). A major aim of this article is to use rigorous methods to shed light on the fluid permeability and other transport properties of models of disordered hyperuniform porous media and to contrast their transport characteristics with those of nonhyperuniform disordered models. In carrying out this investigation, we not only draw from the ideas and results of the emerging field of hyperuniformity, but from homogenization theory, statistical geometry, differential equations (spectrum of Laplace and Stokes operators), and the covering and quantizer problems of discrete geometry.

In Section 2, we define relevant microstructural descriptors and hyperuniformity, including how to measure hyperuniformity. In Section 3, we briefly review the homogenized relations that determine all of the transport properties of interest to us in this work, i.e., $F$, $\tau$, $T_1$ and $\Theta_1$ and $k$, as well as rigorous cross-property relations linking $k$ to the other transport properties. In Section 4, we state the microstructure-dependent formulas that we will employ to estimate the various effective properties. In Section 5, we describe hyperuniform and nonhyperuniform porous-media models that we examine and present their spectral densities and pore-size probability functions. In Section 6, we compute the effective transport properties of a variety of different hyperuniform and nonhyperuniform models of porous media. We also derive a Fourier representation of the classic two-point void upper bound on the fluid permeability that depends on the spectral density. This new formula enables us to infer the salient microstructural features that determine the permeabilities of hyperuniform and nonhyperuniform porous media. We use rigorous bounds on individual effective properties as well as cross-property relations to suggest a new approximate formula for the fluid permeability that provides reasonably accurate permeability predictions of the class of hyperuniform and nonhyperuniform porous media in which the pore space is well connected. In Section 7, we make concluding remarks and discuss problems for future research.

## 2. Definitions of microstructural descriptors and hyperuniformity

Two-phase heterogeneous media abound in Nature and synthetic situations. Examples of such materials include composites and porous media, biological media, foams, polymer blends, granular media, cellular solids and colloids (Torquato, 2002a; Sahimi, 2003). There is a panoply of different statistical descriptors of the microstructure of two-phase media; see Ref. Torquato (2002a) and references therein. The most relevant for the purposes of this paper are the $n$-point correlation functions and pore-size distributions, defined briefly below. We also highlight the hyperuniformity concept that we will apply in subsequent sections.

### 2.1. n-Point Correlation functions

A two-phase random medium is a domain of space $\mathcal{V} \subseteq \mathbb{R}^d$ that is partitioned into two disjoint regions that make up $\mathcal{V}$: a phase 1 region $\mathcal{V}_1$ of volume fraction $\phi_1$ and a phase 2 region $\mathcal{V}_2$ of volume fraction $\phi_2$ (Torquato, 2002a). The phase indicator function $I^{(i)}(\mathbf{x};\omega)$ for a given realization $\omega$ is defined as

$$I^{(i)}(\mathbf{x};\omega) = \begin{cases} 1, & \mathbf{x} \in \mathcal{V}_i, \\ 0, & \mathbf{x} \notin \mathcal{V}_i. \end{cases} \tag{1}$$

The statistical properties of each phase of the system are specified by the countably infinite set of $n$-correlation functions $S_n^{(i)}$, which are

defined by Torquato and Stell (1982), Stoyan et al. (1995), and Torquato (2002a):

$$S_n^{(i)}(\mathbf{x}_1,\ldots,\mathbf{x}_n) = \left\langle \prod_{j=1}^{n} \mathcal{I}^{(i)}(\mathbf{x}_j;\omega) \right\rangle, \tag{2}$$

where angular brackets denote an ensemble average over realizations. The $n$-point correlation function $S_n^{(i)}(\mathbf{x}_1,\ldots,\mathbf{x}_n)$ has a probabilistic interpretation: it gives the probability of finding the ends of the vectors $\mathbf{x}_1,\ldots,\mathbf{x}_n$ all in phase $i$. For this reason, $S_n^{(i)}(\mathbf{x}_1,\ldots,\mathbf{x}_n)$ is sometimes referred to as the *n-point probability function*.

If the medium is statistically homogeneous, $S_n^{(i)}(\mathbf{x}_1,\ldots,\mathbf{x}_n)$ is translationally invariant and, in particular, the one-point correlation function is independent of position and equal to the volume fraction of phase $i$:

$$S_1^{(i)}(\mathbf{x}) = \phi_i, \tag{3}$$

while the two-point correlation function $S_2^{(i)}(\mathbf{r})$ depends on the displacement vector $\mathbf{r} \equiv \mathbf{x}_2 - \mathbf{x}_1$.

For statistically homogeneous media, the two-point correlation function for phase 2 is simply related to that for phase 1 via the expression $S_2^{(2)}(\mathbf{r}) = S_2^{(1)}(\mathbf{r}) - 2\phi_1 + 1$, and hence the *autocovariance* function is given by

$$\chi_{_V}(\mathbf{r}) \equiv S_2^{(1)}(\mathbf{r}) - {\phi_1}^2 = S_2^{(2)}(\mathbf{r}) - {\phi_2}^2, \tag{4}$$

which we see is the same for phase 1 and phase 2. At the extreme limits of its argument, $\chi_{_V}$ has the following asymptotic behavior

$$\chi_{_V}(\mathbf{r}=0) = \phi_1\phi_2, \quad \lim_{|\mathbf{r}|\to\infty} \chi_{_V}(\mathbf{r}) = 0, \tag{5}$$

the latter limit applying when the medium possesses no long-range order. If the medium is statistically homogeneous and isotropic, then the autocovariance function $\chi_{_V}(\mathbf{r})$ depends only on the magnitude of its argument $r = |\mathbf{r}|$, and hence is a radial function. In such instances, its slope at the origin is directly related to the *specific surface* $s$ (interface area per unit volume); specifically, we have in any space dimension $d$, the asymptotic form Torquato (2002a),

$$\chi_{_V}(\mathbf{r}) = \phi_1\phi_2 - \beta(d)s\,|\mathbf{r}| + \mathcal{O}(|\mathbf{r}|^2), \tag{6}$$

where

$$\beta(d) = \frac{\Gamma(d/2)}{2\sqrt{\pi}\Gamma((d+1)/2)} \tag{7}$$

and $\Gamma(x)$ is the gamma function.

The nonnegative spectral density $\tilde{\chi}_{_V}(\mathbf{k})$, which can be obtained from scattering experiments (Debye and Bueche, 1949; Debye et al., 1957), is the Fourier transform of $\chi_{_V}(\mathbf{r})$, i.e.,

$$\tilde{\chi}_{_V}(\mathbf{k}) = \int_{\mathbb{R}^d} \chi_{_V}(\mathbf{r})\, e^{-i\mathbf{k}\cdot\mathbf{r}} d\mathbf{r} \geq 0, \text{ for all } \mathbf{k}. \tag{8}$$

For a general statistically homogeneous two-phase medium, the spectral density must obey the following sum rule

$$\frac{1}{(2\pi)^d} \int_{\mathbb{R}^d} \tilde{\chi}_{_V}(\mathbf{k})\, d\mathbf{k} = \chi_{_V}(\mathbf{r}=0) = \phi_1\phi_2. \tag{9}$$

This follows immediately from the Fourier representation of the autocovariance function, i.e.,

$$\chi_{_V}(\mathbf{r}) = \frac{1}{(2\pi)^d} \int_{\mathbb{R}^d} \tilde{\chi}_{_V}(\mathbf{k})\, e^{i\mathbf{k}\cdot\mathbf{r}} d\mathbf{k}. \tag{10}$$

For isotropic media, the spectral density only depends on $k = |\mathbf{k}|$ and, as a consequence of (6), its decay in the large-$k$ limit is controlled by the exact following power-law form:

$$\tilde{\chi}_{_V}(\mathbf{k}) \sim \frac{\gamma(d)\, s}{k^{d+1}}, \quad k \to \infty, \tag{11}$$

where

$$\gamma(d) = 2^d\, \pi^{(d-1)/2} \Gamma((d+1)/2)\beta(d) \tag{12}$$

is a $d$-dimensional constant and $\beta$(d) is given by (7).

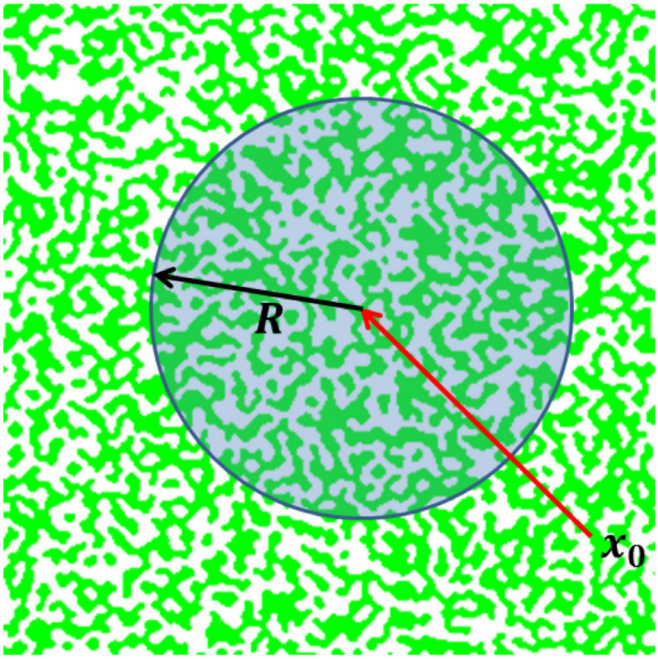


**Fig. 2.** A schematic indicating a circular observation window of radius $R$ that is centered at position $\mathbf{x}_0$ in a disordered two-phase medium; one phase is depicted as a green region and the other phase as a white region. The phase volume fractions within the window will fluctuate as the window position $\mathbf{x}_0$ is varied. (For interpretation of the references to colour in this figure legend, the reader is referred to the web version of this article.)

### 2.2. Volume-fraction fluctuations and hyperuniformity

A hyperuniform point process in $d$-dimensional Euclidean space $\mathbb{R}^d$ is one in which the variance associated with the number of points within a spherical observation window of radius $R$ grows more slowly than $R^d$ (i.e., window volume) in the large-$R$ limit (Torquato and Stillinger, 2003). Equivalently, it is one in which the structure factor

$$S(\mathbf{k}) \equiv 1 + \rho\tilde{h}(\mathbf{k}) \tag{13}$$

tends to zero as the wavenumber $k \equiv |\mathbf{k}|$ tends to zero (Torquato and Stillinger, 2003), where $\tilde{h}(\mathbf{k})$ is the Fourier transform of the total correlation function $h(\mathbf{r}) = g_2(\mathbf{r}) - 1$ and $g_2(\mathbf{r})$ is the standard pair correlation function. Typical disordered systems, such as liquids and structural glasses, possess local number variances that grow as the window volume, that is, proportional to $R^d$. All perfect crystals and many perfect quasicrystals are hyperuniform. Moreover, there are special disordered systems that are hyperuniform. They are exotic ideal states of amorphous matter have attracted great attention because they have characteristics that lie between a crystal and liquid; they are like perfect crystals in the way they suppress large-scale density fluctuations and yet are like liquids or glasses in that they are statistically isotropic with no Bragg peaks and hence lack any conventional long-range order (Torquato, 2018a). These unusual attributes can endow disordered hyperuniform systems with novel optical, mechanical and transport properties (Torquato, 2018a; Ding et al., 2018).

The hyperuniformity concept was generalized to the case of two-phase heterogeneous materials (Zachary and Torquato, 2009). Here the phase volume fraction fluctuates within a finite-sized spherical window of radius $R$ (see Fig. 2), which can be characterized by the local volume-fraction variance $\sigma_{_V}^2(R)$, which in turn can be related to the autocovariance function as follows (Lu and Torquato, 1990):

$$\sigma_{_V}^2(R) = \frac{1}{v_1(R)} \int_{\mathbb{R}^d} \chi_{_V}(\mathbf{r})\alpha(r;R)d\mathbf{r}, \tag{14}$$

where $\alpha(r; R)$ is intersection volume of two identical spheres of radius $R$ (scaled by the volume of a sphere) whose centers are separated by a distance $r$, which is known analytically in any space dimension Torquato and Stillinger (2003, 2006). The alternative Fourier representation of $\sigma_V^2(R)$ was obtained in Ref. Zachary and Torquato (2009):

$$\sigma_V^2(R) = \frac{1}{v_1(R)(2\pi)^d} \int_{\mathbb{R}^d} \tilde{\chi}_V(\mathbf{k}) \tilde{\alpha}(k; R) d\mathbf{k}, \tag{15}$$

where $\tilde{\alpha}(k; R) = (4\pi)^{d/2}\Gamma(1 + d/2)J_{d/2}^2(kR)/k^d$ is the Fourier transform of $\alpha(r; R)$ (Torquato and Stillinger, 2003; Zachary and Torquato, 2009) and $J_\nu(x)$ is the Bessel function of the first kind of order $\nu$.

For typical disordered two-phase media, the variance $\sigma_V^2(R)$ for large $R$ goes to zero like $R^{-d}$ (Lu and Torquato, 1990; Quintanilla and Torquato, 1997) and hence the value of $R$ at which the product $\sigma_V^2(R)\, R^d$ first effectively reaches its asymptote provides a linear measure of the representative elementary volume. However, for hyperuniform disordered two-phase media, $\sigma_V^2(R)$ goes to zero asymptotically more rapidly than the inverse of the window volume, i.e., faster than $R^{-d}$, which is equivalent to the following condition on the spectral density (defined in Section 2):

$$\lim_{|\mathbf{k}|\to 0} \tilde{\chi}_V(\mathbf{k}) = 0. \tag{16}$$

*Stealthy hyperuniform* two-phase media are a subclass of hyperuniform systems in which $\tilde{\chi}_V(\mathbf{k})$ is zero for a range of wave vectors around the origin, i.e.,

$$\tilde{\chi}_V(\mathbf{k}) = 0 \text{ for } 0 \le |\mathbf{k}| \le K, \tag{17}$$

where $K$ is some positive number. As in the case of hyperuniform point configurations (Torquato and Stillinger, 2003; Zachary and Torquato, 2009; 2011; Torquato, 2018a), there are three different scaling regimes (classes) when the spectral density goes to zero with the power-law form $\tilde{\chi}_V(\mathbf{k}) \sim |\mathbf{k}|^\alpha$ that describe the associated large-$R$ behaviors of local volume-fraction variance:

$$\sigma_V^2(R) \sim \begin{cases} R^{-(d+1)}, & \alpha > 1 \quad \text{(Class I)} \\ R^{-(d+1)} \ln R, & \alpha = 1 \quad \text{(Class II)}, \\ R^{-(d+\alpha)}, & 0 < \alpha < 1 \quad \text{(Class III)} \end{cases} \tag{18}$$

where the exponent $\alpha$ is a positive constant. Thus, the linear measure of the representative elementary volume for a hyperuniform medium will depend on the hyperuniformity class (scaling).

Class I is the strongest hyperuniformity class, which includes all perfect periodic packings as well as some disordered packings, such as disordered stealthy packings described in Section 5.2.2. We call a *packing* in $\mathbb{R}^d$ a collection of nonoverlapping particles (Torquato, 2018b). While all class I have local volume-fraction variances that scale as $R^{-(d+1)}$ for large $R$, the coefficient $\overline{B}_V$ multiplying $R^{-(d+1)}$ is different among them and hence $\overline{B}_V$ provides a *hyperuniformity* order metric that can be used to rank order different structures according to degree that they suppress large-scale local volume-fraction fluctuations (Torquato and Stillinger, 2003; Zachary and Torquato, 2009; Torquato, 2018a; Torquato et al., 2015). These previous results indicate that the body-centered cubic (BCC) lattice packing in three dimensions has the smallest hyperuniformity order metric $\overline{B}_V$ (most ordered with respect to this metric) when compared to other packings at the same number density and packing fraction. Fig. 3 schematically shows the ranking of this order metric for some selected packings. We will see that the BCC packing plays a special role in various problems described in this paper.

In the case of a packing of identical spheres of radius $a$ at number density $\rho$, the spectral density $\tilde{\chi}_V(\mathbf{k})$ is directly related to the structure factor $S(\mathbf{k})$ of the sphere centers (Torquato, 2002a; 2016a):

$$\tilde{\chi}_V(\mathbf{k}) = \rho\, \tilde{m}^2(k; a)\, S(\mathbf{k}), \tag{19}$$

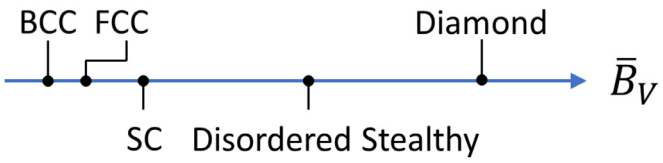


**Fig. 3.** A schematic that shows the ranking of some selected hyperuniform packings, including the BCC, FCC, SC, diamond and disordered stealthy packing, according to the order metric $\overline{B}_V$. Note that the BCC packing is the minimizer and the disordered stealthy packing can suppress volume-fraction fluctuations to a greater degree than that of the crystal diamond packing. The reader is referred to Refs. Torquato and Stillinger (2003); Zachary and Torquato (2009); Torquato (2018a) and Torquato et al. (2015) for the quantitative basis of the rankings depicted here for these chosen structures.

where $\tilde{m}(k; a)$ is the Fourier transform of a sphere indicator function given by

$$\tilde{m}(k; a) = \left(\frac{2\pi a}{k}\right)^{d/2} J_{d/2}(ka). \tag{20}$$

Asymptotic analysis of (20) for large values of $k$ and comparison to relation (11) reveals the expected result for the specific surface of any packing of identical spheres, namely,

$$s = \frac{3\phi_2}{a}, \tag{21}$$

where $\phi_2$ is the packing fraction (fraction of space covered by the spheres), which is given by

$$\phi_2 = \rho v_1(a), \tag{22}$$

and

$$v_1(a) = \frac{\pi^{d/2} a^d}{\Gamma(1 + d/2)} \tag{23}$$

is the volume of a $d$-dimensional sphere of radius $a$.

### 2.3. Pore-Size distribution

We also characterize the pore phase by determining the probability $F(\delta)$ that a randomly placed sphere of radius $\delta$ centered in the pore space $\mathcal{V}_1$ lies entirely in $\mathcal{V}_1$. By definition, $F(0) = 1$ and $F(\infty) = 0$. The quantity $F(\delta)$ is the complementary cumulative distribution function associated with the corresponding pore-size probability density function $P(\delta) = -\partial F(\delta)/\partial\delta$. At the extreme values of $P(\delta)$, we have that $P(0) = s/\phi_1$ and $P(\infty) = 0$. The $n$th moment of the pore-size probability density is defined by Torquato (2002a)

$$\langle \delta^n \rangle \equiv \int_0^\infty \delta^n P(\delta)\, d\delta = n \int_0^\infty \delta^{n-1} F(\delta)\, d\delta\,. \tag{24}$$

We will be particularly interested in the *mean pore size* $\langle\delta\rangle$ and the *second moment* $\langle\delta^2\rangle$:

$$\langle \delta \rangle = \int_0^\infty F(\delta)\, \mathrm{d}\delta\,, \tag{25}$$

$$\langle \delta^2 \rangle = 2 \int_0^\infty \delta\, F(\delta)\, \mathrm{d}\delta\,. \tag{26}$$

We will see that these characteristic length scales of the pore phase can be related to certain diffusion properties of the porous medium. Note that the pore-size probability function $F(\delta)$ can be easily extracted from 3D digitized images of real porous media (Coker et al., 1996).

For models of porous media consisting of distributions of identical spheres of radius $a$ (nonoverlapping or not), the complementary cumulative pore-size distribution $F(\delta)$ is trivially related to the so-called *void exclusion probability* $E_V(r)$ via the relation (Torquato, 2002a)

$$F(\delta) = \frac{E_V(\delta + a)}{\phi_1}, \qquad \delta \ge 0\,. \tag{27}$$

The exclusion probability $E_V(r)$ gives the probability that a test sphere of radius $r$ that is placed randomly in the medium does not contain any sphere center. The quantity

$$H_V(r) = -\frac{\partial E_V(r)}{\partial r}. \tag{28}$$

is the associated "void" nearest-neighbor probability density function.

## 3. Local differential equations and effective transport properties

### 3.1. Formation factor and tortuosity of the pore space

Consider a porous medium whose pore space $\mathcal{V}_1$ is filled with an electrically conducting fluid of conductivity $\sigma_1$ and a solid phase that is perfectly insulating ($\sigma_2 = 0$). At steady-state, the scaled electric field $\mathbf{E}$ (actual electric field divided by the modulus of the ensemble-averaged electric field) satisfies

$$\nabla \cdot \mathbf{E} = 0 \quad \text{in } \mathcal{V}_1, \tag{29}$$

$$\nabla \times \mathbf{E} = 0 \quad \text{in } \mathcal{V}_1, \tag{30}$$

$$\mathbf{E} \cdot \mathbf{n} = 0 \quad \text{on } \partial\mathcal{V}_1, \tag{31}$$

where $\mathbf{n}$ is the unit outward normal at the pore-solid interface $\partial\mathcal{V}_1$. Homogenization theory provides the conditions under which the scaled effective conductivity of the porous medium $\sigma_e/\sigma_1$ has the well-known "energy" representation:

$$\sigma_e/\sigma_1 = \mathcal{F}^{-1} = \langle \mathbf{E} \cdot \mathbf{E} \rangle, \tag{32}$$

where $\mathcal{F}$ denotes the *formation factor*, which is the commonly employed designation for $\sigma_1/\sigma_e$, and angular brackets denote an ensemble average. The formation factor $\mathcal{F}$ is a measure of the *tortuosity* of the *entire* pore space, including topologically connected parts of the pore space as well as disconnected portions (e.g., isolated pores). If the pore space does not percolate, then $\mathcal{F}$ is unbounded or, equivalently, $\sigma_e/\sigma_1 = 0$. Roughly speaking, the formation factor $\mathcal{F}$ quantifies the degree of "windiness" for electrical transport pathways across a macroscopic sample.

### 3.2. Diffusion (NMR) relaxation problem and effective time scales

Nuclear magnetic resonance (NMR) relaxation times of porous media provide useful probes of the pore-phase microstructure (Mitra et al., 1992; 1993; Bergman and Dunn, 1994; Sen and Hürlimann, 1994; Øren et al., 2002). Let $m(\mathbf{r}, \mathbf{t})$ denote the magnetization density at local position $\mathbf{r}$ and time $t$ inside the pore phase $\mathcal{V}_1$ in which there are generally paramagnetic impurities at the pore-solid interface $\partial\mathcal{V}$ that will tend to demagnetize the diffusing particle when it strikes the interface. The magnetization density obeys the time-dependent diffusion equation in the pore region $\mathcal{V}_1$

$$\frac{\partial m}{\partial t} = D \triangle m + m_o \delta(t) \text{ in } \mathcal{V}_1, \tag{33}$$

$$D\frac{\partial m}{\partial n} + \kappa m = 0 \text{ on } \partial\mathcal{V}. \tag{34}$$

Here $D$ is the diffusion coefficient, $\kappa$ is the surface rate constant, $\triangle$ is the Laplacian operator, $m_o$ is the initial magnetization density, and $\delta(t)$ is the Dirac delta function. In the *diffusion-controlled* regime, the diffusing species takes a long time to diffuse to the pore–trap interface relative to the characteristic time associated with the surface reaction. For infinite surface reaction ($\kappa = \infty$), the traps are perfect absorbers, and thus the interface condition is of the *Dirichlet* kind, with $m = 0$. On the other hand, in the *reaction-controlled* regime, the characteristic time associated with surface reaction is large compared with the diffusion time to the pore–trap interface. For vanishing surface reaction ($\kappa = 0$), the traps are perfect reflectors, and hence the interface condition is of the *Neumann* kind, with $\partial m/\partial n = 0$.

The solution of (33) and (34) can be expressed as an expansion in orthonormal functions (Torquato and Avellaneda, 1991). The diffusion relaxation times $T_n$ are inversely related to the eigenvalues $\lambda_n$ by $T_n = 1/(D\lambda_n)$. The survival probability $S(t)$, which gives the fraction of Brownian particles that survive until time $t$, is a monotonically decreasing function of time that is explicitly known to be an infinite sum involving the entire spectrum of relaxation times (Torquato and Avellaneda, 1991). The long-time behavior of the survival probability $S(t)$ is determined by the largest or *principal* relaxation time $T_1$, which in turn is intimately linked to pore-size fluctuations.

Using homogenization theory (Rubinstein and Torquato, 1988), it was shown that the *mean survival time* $\tau$, which is defined by

$$\tau = \frac{\langle u \rangle}{\phi_1 D}, \tag{35}$$

where $u$ is the scaled magnetization density satisfying the steady-state diffusion equation:

$$\triangle u = -1 \text{ in } \mathcal{V}_1, \tag{36}$$

$$\frac{\partial u}{\partial n} + \kappa u = 0 \text{ on } \partial\mathcal{V}. \tag{37}$$

The mean survival time gives the average time for a Brownian particle to survive before it gets trapped and, interestingly, can also be obtained from NMR relaxation, since it is the area under the survival time curve (Torquato and Avellaneda, 1991), i.e.,

$$\tau = \int_0^\infty S(t)dt. \tag{38}$$

The times $\tau$ and $T_1$ are intimately linked to characteristic length scales of the pore region. As in the case of the formation factor $\mathcal{F}$, they account for the entire pore space, whether topologically connected or not. Whereas the mean survival time $\tau$ is determined by the "average pore size," the *principal* (largest) relaxation time $T_1$ is governed by diffusion occurring in the largest pores in the system. Torquato and Avellaneda (1991) have shown that the mean survival time $\tau$ is bounded from above and below in terms of the principal relaxation $T_1$. For example, the upper bound on $\tau$ is given by

$$\tau \leq T_1. \tag{39}$$

### 3.3. Fluid permeability

Homogenization theory was applied to show that the isotropic fluid permeability $k$ arising in Darcy's law of a random porous medium can be expressed as the ensemble average of a scaled velocity field (Rubinstein and Torquato, 1989). Specifically, the permeability is given by

$$k = \langle \mathbf{w} \cdot \mathbf{e} \rangle, \tag{40}$$

where $\mathbf{w}$ is scaled vector velocity field that satisfies

$$\triangle \mathbf{w} = \boldsymbol{\nabla}\pi - \mathbf{e} \text{ in } \mathcal{V}_1, \tag{41}$$

$$\boldsymbol{\nabla} \cdot \mathbf{w} = 0 \text{ in } \mathcal{V}_1, \tag{42}$$

$$\mathbf{w} = 0 \text{ on } \partial\mathcal{V}, \tag{43}$$

$\pi$ is a scaled pressure field and $\mathbf{e}$ is a unit vector in the direction of the applied pressure gradient.

Now consider the unsteady Stokes equations for the fluid velocity vector field $\mathbf{v}(\mathbf{r}, t)$ at position $\mathbf{r}$ and time $t$ in $\mathcal{V}_1$:

$$\frac{\partial \mathbf{v}}{\partial t} = -\nabla\left(\frac{p}{\rho}\right) + \nu \triangle \mathbf{v} + v_0 \mathbf{e}\, \delta(t) \text{ in } \mathcal{V}_1 \tag{44}$$

$$\nabla \cdot \mathbf{v} = 0 \text{ in } \mathcal{V}_1 \tag{45}$$

$$\mathbf{v} = 0 \text{ on } \partial\mathcal{V}. \tag{46}$$

Here $p(\mathbf{r}, t)$ is the pressure, $\rho$ is the constant fluid density, $\nu$ is the kinematic viscosity, $\nu_0$ is a constant, and $\mathbf{e}$ is an arbitrary unit vector. Avellaneda and Torquato (1991) used the solutions of (44)–(46), which can be expressed as a sum of normal modes, to derive the first rigorous relation connecting the fluid permeability $k$ to the formation factor of the porous medium and a length scale $\mathcal{L}$ that is determined by the eigenvalues of the Stokes operator. Specifically, the fluid permeability is exactly given by

$$k = \frac{\mathcal{L}^2}{\mathcal{F}}, \tag{47}$$

where $\mathcal{L}$ is a certain weighted sum over the *viscous relaxation times* $\Theta_n$ associated with the time-dependent Stokes equations (i.e., inversely proportional to the eigenvalues of the Stokes operator). The reader should note that the length scale $\mathcal{L}$ appearing in (47) absorbs a factor of 8 compared to the definition $L$ given in Ref. Avellaneda and Torquato (1991); specifically, $\mathcal{L} = L/8$. Avellaneda and Torquato (1991) also showed how to explicitly relate the spectrum $\Theta_n$ to the *dynamic* fluid permeability $k(\omega)$, where $\omega$ is the frequency associated with an imposed oscillatory pressure gradient.

## 4. Microstructure-Dependent effective property estimates

### 4.1. Formation factor

Rigorous upper and lower bounds have been derived on the effective conductivity $\sigma_e$ of two-phase media that incorporate various $n$-point correlation functions; see Refs. Milton (2002) and Torquato (2002a) and references therein. In the special case of a conducting fluid of phase conductivity $\sigma_1$ and a perfectly insulating solid phase ($\sigma_2 = 0$), one can trivially extract the formation factor $\mathcal{F}$ defined by (32). For example, a tight lower bound on $\mathcal{F}$ for any such 3D porous medium that accounts for up to four-point correlation function information can be obtained from Ref. Torquato (1985):

$$\mathcal{F} \geq \frac{1 + \frac{1}{2}\frac{\gamma_2}{\zeta_2} - \frac{1}{2}\zeta_2 + \left(\frac{1}{2} + \frac{1}{2}\zeta_2 + \frac{1}{4}\frac{\gamma_2}{\zeta_2}\right)\phi_2}{1 + \frac{1}{2}\frac{\gamma_2}{\zeta_2} - \frac{1}{2}\zeta_2 + \left(-1 + \frac{1}{2}\zeta_2 - \frac{1}{2}\frac{\gamma_2}{\zeta_2}\right)\phi_2}, \tag{48}$$

where the three-point microstructural parameter $\zeta_2$ is a certain weighted integral that involves the correlation functions $S_1^{(2)}$, $S_2^{(2)}$ and $S_3^{(2)}$ of phase 2 [cf. (2)] and the four-point microstructural parameter $\gamma_2$ is a certain weighted integral that involves the correlation functions $S_1^{(2)}$, $S_2^{(2)}$, $S_3^{(2)}$ and $S_4^{(2)}$. The reader is referred to Ref. Torquato (1985) for detailed discussions of these parameters. The corresponding upper bound on $\mathcal{F}$ diverges to infinity because it corresponds to microstructures in which the pore space is fully topologically disconnected.

For a wide class of ordered and disordered packings in which the particles form phase 2, theoretical arguments were presented to show that the four-point parameter is equal to zero, to a very good approximation. This conclusion together with (48) led to the following approximation for such media in terms of the three-point parameter $\zeta_2 \in [0, 1]$:

$$\mathcal{F} \approx \frac{2 + \phi_2 - \phi_1\zeta_2}{\phi_1(2 - \zeta_2)}. \tag{49}$$

The high predictive power of this approximation and its more general counterpart that applies to the effective conductivity $\sigma_e$ for any phase contrast ratio $\sigma_2/\sigma_1$ (Torquato, 1985) has been validated by computer simulations of the effective conductivity of a variety of ordered and disordered dispersions of spheres in a matrix (Torquato, 1985; Kim and Torquato, 1991; Robinson and Friedman, 2005; Gillman and Matouš, 2014; Gillman et al., 2015; Nguyen et al., 2016).

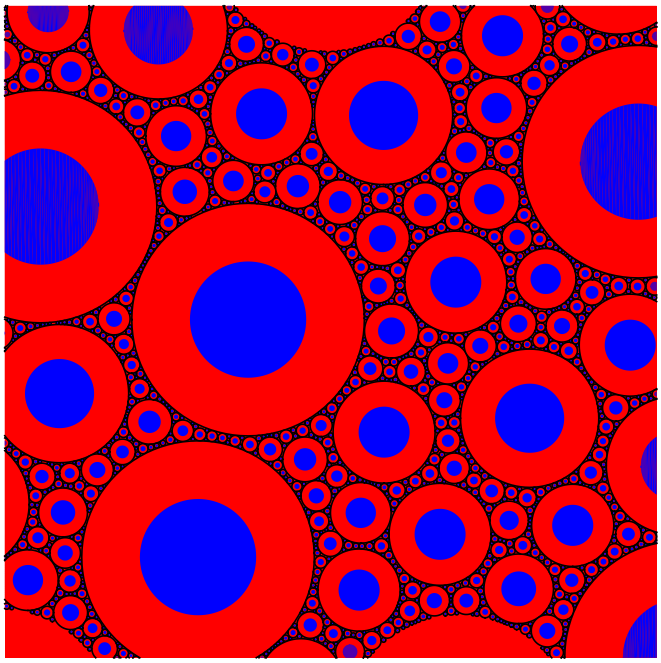

**Fig. 4.** Schematic of the optimal 2D multiscale "coated-cylinders" model that realize the Hashin-Shtrikman bounds. In the case when phase 1 is conducting and phase 2 is perfectly insulating, phase 2 is the dispersed phase (shown in blue). (For interpretation of the references to colour in this figure legend, the reader is referred to the web version of this article.)

Note that when $\zeta_2 = 0$, relation (49) reduces to the optimal Hashin-Shtrikman lower bound on $\mathcal{F}$ given the volume fraction and two-point correlation function information (Hashin and Shtrikman, 1962; Torquato, 2002a). The Hashin-Shtrikman upper and lower bounds on the effective conductivity for arbitrary phase contrast ratios $\sigma_2/\sigma_1$ are optimal because their effective conductivities are exactly realized by certain multiscale dispersions, including the "coated-spheres" model in three dimensions and the "coated-cylinders" model in two dimensions, which is depicted in Fig. 4. Such two-phase media consist of composite spheres, each of which is composed of a spherical core of one phase (dispersed phase) that is surrounded by a concentric spherical shell of the other phase such that the fraction of space occupied by the dispersed phase is equal to its overall phase volume fraction. The composite spheres fill all space, implying that their sizes range down to the infinitesimally small. Interestingly, it has recently been proved that these highly degenerate optimal Hashin-Shtrikman multiscale dispersions are hyperuniform (Kim and Torquato, 2019b; 2019a) which apparently is an important structural attribute to attain optimal effective conductivities and elastic properties (Hashin and Shtrikman, 1963).

### 4.2. NMR Time scales

The mean survival time $\tau$ for a general porous medium with porosity $\phi_1 = 1 - \phi_2$ is rigorously bounded from below according to Torquato and Avellaneda (1991)

$$\tau \geq \frac{\langle\delta\rangle^2}{D} + \frac{\phi_1}{\kappa s}. \tag{50}$$

where $\langle\delta\rangle$ is the mean pore size defined by (25) and $s$ is the specific surface. In the diffusion-controlled limit in which $\kappa/D \to \infty$, this lower bound reduces to one first derived by Prager (1963).

The mean survival time is bounded from above by the following weighted integral of the autocovariance function (Torquato and Rubinstein, 1989):

$$D\tau \le \frac{1}{\phi_1 \phi_2^2}\,\ell_P^2, \tag{51}$$

where

$$\ell_P^2 = \int_0^\infty \chi_V(r)\, r dr. \tag{52}$$

The inequality (51) has been referred as the two-point "void" upper bound on $\tau$ Torquato and Rubinstein (1989).

The two-point void bound has been generalized to treat two-dimensional media as well as dimensions higher than three (Torquato, 2002a). It has been shown that for the hyperuniform "coated-spheres" model for $d = 3$ and "coated-cylinders" model for $d = 2$ discussed in Section 4.1 and depicted in Fig. 4, realize the corresponding two-point void upper bound and hence maximize the mean survival times among all microstructures that share the same porosities $\phi_1$ and and pore length scales $\ell_P$ (Torquato and Pham, 2004). For general porous media, the two-point "interfacial-surface" bound on the mean survival time (Doi, 1976; Rubinstein and Torquato, 1988) provides an even tighter upper bound on $\tau$, which is briefly described in the Appendix, including its new Fourier representation.

Rigorous lower bounds on the principal relaxation time $T_1$ have been derived for any value of the surface rate constant $\kappa$. In the diffusion-controlled regime, asymptotic analysis of this lower bound yields

$$T_1 \ge \frac{\langle \delta^2 \rangle}{D} + \frac{3\phi_1 \langle \delta \rangle^2}{4\kappa\, s \langle \delta^2 \rangle}, \tag{53}$$

where $\langle \delta^2 \rangle$ is the second moment of the pore-size function defined by (26). Note that in the diffusion-controlled limit, this inequality reduces to the result due to Prager (1963).

### 4.3. Fluid permeability

#### 4.3.1. Rigorous bounds

The two-point "void" upper bound on the fluid permeability of a general porous medium with porosity $\phi_1 = 1 - \phi_2$ is given by

$$k \le \frac{2}{3\phi_2^2}\,\ell_P^2, \tag{54}$$

where $\ell_P$ is exactly the same length scale (52) that arises in the analogous two-point void bound (51) on the mean survival time $\tau$. The two-point void bound (54) was originally derived by Prager (1961) with an incorrect constant prefactor. This prefactor was subsequently corrected by Berryman and Milton (1985) and Rubinstein and Torquato (1989) using different variational approaches.

The two-point void bound (54) on the fluid permeability has been generalized to treat two-dimensional media as well as dimensions higher than three (Torquato, 2002a). It is noteworthy that for the hyperuniform "coated-cylinders" model in two dimensions (see Fig. 4), the two-point void upper bound maximizes the permeability among all microstructures that share the same porosity $\phi_1$ and pore length scale $\ell_P$ (Torquato and Pham, 2004). For general porous media, the two-point "interfacial-surface" bound on the fluid permeability (Doi, 1976; Rubinstein and Torquato, 1988) provides an even tighter upper bound on $k$, which is briefly described in the Appendix, including its new Fourier representation.

#### 4.3.2. Rigorous cross-Property relations

Torquato (1990) derived the first rigorous relation connecting the fluid permeability tensor to an effective diffusion parameter, namely, the mean survival time $\tau$ associated with steady-state diffusion of "reactants" in the fluid region of a porous medium containing perfectly absorbing pore walls, i.e., infinite surface rate constant $\kappa$ (see Section 3.2). This takes the form of an inequality and its scalar version, valid for arbitrary isotropic media, bounds the fluid permeability $k$ from above in terms of $\tau$: is given by

$$k \le D\,\tau\,\phi_1\,. \tag{55}$$

where $D$ is the diffusion coefficient and $\phi_1$ is the porosity. The upper bound (55) becomes an equality for transport interior to parallel tubes of arbitrary cross-section (in the direction of the tubes). This cross-property bound is relatively tight for flow around dilute arrays of obstacles, but not for a high concentration of obstacles. The latter instance highlights the fact that the mean survival time $\tau$ cannot distinguish between pore channels involving significant momentum transport from those involving little or no momentum transport. Moreover, for any *disconnected* pore space, $k$ is zero while $\tau$ is nonzero. Note that in the more general case of partially reflecting pore walls ($\kappa < \infty$), $\tau(\kappa) > \tau \equiv \tau(\infty)$, and hence one has the generally weaker inequality

$$k \le D\,\tau(\kappa)\,\phi_1\,. \tag{56}$$

Using the characteristics of the Stokes operator, Avellaneda and Torquato (1991) derived sharper cross-property bounds relating the permeability to viscous and diffusion time scales as well as the formation factor. Specifically, they proved that

$$k \le \frac{\nu \Theta_1}{\mathcal{F}} \tag{57}$$

where $\nu$ is the kinematic viscosity and $\Theta_1$ is the principal (largest) *viscous* relaxation time, as discussed in Section 3.3. They showed that since $\nu\Theta_1 \le DT_1$, where $T_1$ is the principal (largest) *diffusion* relaxation time (see Section 3.2), the previous bound leads to the following somewhat weaker bound for arbitrary $\kappa$:

$$k \le \frac{DT_1}{\mathcal{F}}\,. \tag{58}$$

It immediately follows from (47) and (58) that exact length scale $\mathcal{L}$ is bounded from above in terms of $T_1$ according to

$$\mathcal{L}^2 \le DT_1\,. \tag{59}$$

As noted earlier, $T_1$ can be obtained from NMR experiments. Thus, via inequality (58), the permeability is related to purely diffusional transport parameters, i.e., $T_1$ and $\mathcal{F}$, which can be readily measured.

It has been shown that (58) provides relatively accurate estimates of the permeability of versatile grain-consolidation models (Torquato and Kim, 1992). Since $T_1$ is closely related to the second moment of the pore-size function [see (53)], the accuracy of the estimate (58) highlights the importance of the second moment $\langle \delta^2 \rangle$ of the pore-size probability density function in determining the square of the exact length scale $\mathcal{L}$ and hence the fluid permeability of certain porous media, as will be elaborated below.

## 5. Model microstructures and their structural characteristics

We study and characterize a variety of different models of hyperuniform and nonhyperuniform porous media: ordered and disordered packings of spheres, overlapping spheres, and Debye random media. Of particular interest is the spectral density $\tilde{\chi}_V(\mathbf{k})$ and pore-size probability function $F(\delta)$ for these models. In most of the cases, these statistical descriptors can be obtained as closed-form analytical expressions.

### 5.1. Nonhyperuniform disordered models

We study three different nonhyperuniform disordered model microstructures: equilibrium packings, overlapping spheres, and Debye random media.

#### 5.1.1. Equilibrium packings

Equilibrium (Gibbs) ensembles of identical hard spheres of radius $a$ Hansen and McDonald (1986) and Torquato (2018b) are examined. In particular, we consider such disordered packings along the stable disordered fluid branch in the phase diagram (Torquato, 2002a; 2018b). All such states are nonhyperuniform.

#### 5.1.2. Overlapping spheres

Systems of particles whose centroids are uncorrelated (Poisson distributed) that can fully overlap are useful models of heterogeneous media (Weissberg, 1963; Torquato, 2002a). Here we focus on the case in which the particles are identical spheres of radius $a$ at number density $\rho$, which we henceforth refer to as *overlapping spheres*. It is well-known that the autocovariance function of identical overlapping spheres in three dimensions is given by Weissberg (1963) and Torquato (2002a)

$$\chi_V(r) = \exp\left[-\eta\left(1 + \frac{3r}{4a} - \frac{r^3}{16a^3}\right)\right] - \exp(-2\eta) \tag{60}$$

for $r \le 2a$ and zero otherwise, where $\eta = \rho 4\pi a^3/3 = -\ln \phi_1$ is a reduced density, and its specific surface is

$$s = \frac{3\,\phi_1\,\eta}{a}. \tag{61}$$

It is noteworthy that the particle phase percolates for $0.29 \le \phi_2 \le 1$ (Rintoul and Torquato, 1997), while the pore phase percolates for $0 \le \phi_2 \le 0.97$ (Elam et al., 1984; Rintoul, 2000). Thus, the overlapping-spheres model is bicontinuous (both phases simultaneously percolate) for $0.29 \le \phi_2 \le 0.97$.

#### 5.1.3. Debye random media

Debye et al. Debye et al. (1957) hypothesized that the following autocovariance function characterizes isotropic random media in which the phases form domains of "random shape and size":

$$\chi_V(r) = \phi_1\phi_2 \exp(-r/a), \tag{62}$$

where $a$ is a characteristic length scale. However, many years passed since the publication of this work before it was shown that such autocovariances are actually realizable by two-phase media. In two dimensions, it was shown that Debye random media are realizable (Stoyan et al., 1995; Yeong and Torquato, 1998a). Theoretical analyses indicate that such media are realizable in three and higher dimensions (Jiao et al., 2007), but no such explicit constructions have heretofore been identified. Motivated by the implications of our analysis of rigorous permeability estimates in the present work, we provide a 3D realization of a Debye random medium; see Section 6.3.

The Taylor expansion of (62) about $r = 0$ and comparison to (6) reveals that the specific surface $s$ of a Debye random medium in any space dimension is given by

$$s = \frac{\phi_1\,\phi_2}{\beta(d)\,a}. \tag{63}$$

For $d = 3$, our main interest in this paper, this formula yields

$$s = \frac{4\,\phi_1\,\phi_2}{a}. \tag{64}$$

### 5.2. Hyperuniform model microstructures

We also consider hyperuniform packings of identical spheres of radius $a$ with packing fraction $\phi_2$, including ordered and disordered varieties.

#### 5.2.1. Lattice packings

We study nonoverlapping spheres arranged on the sites of simple cubic (SC), face-centered cubic (FCC) and body-centered cubic (BCC) lattices (Ashcroft and Mermin, 1976; Chaikin and Lubensky, 1995; Conway and Sloane, 1998). Such ordered packings which are necessarily hyperuniform and stealthy (Torquato and Stillinger, 2003; Torquato et al., 2015). Such idealized packing models are useful, since their transport properties can be determined exactly, in principle.

Subsequently, we show that the BCC lattice, which is known to be optimal for various problems that arise in many-body physics (Torquato and Stillinger, 2003) and discrete geometry (Conway and Sloane, 1998; Torquato, 2010), has a special status in the case of fluid permeability when the sites of the BCC lattice are decorated with identical nonoverlapping spheres. For example, the BCC lattice is believed to be the point configuration that minimizes a certain measure of large-scale density fluctuations (Torquato and Stillinger, 2003). Moreover, the BCC lattice provides the best known *covering* in three-dimensional space $\mathbb{R}^3$ (Conway and Sloane, 1998; Torquato, 2010). The covering problem asks for the point configuration in $d$-dimensional Euclidean space $\mathbb{R}^d$ that minimizes the radius of overlapping spheres circumscribed around each of the points required to cover $\mathbb{R}^d$. Finally, the BCC lattice also provides the best known *quantizer* in $\mathbb{R}^3$ (Conway and Sloane, 1998; Torquato, 2010; Klatt et al., 2019). The quantizer problem is concerned with finding the point configuration in $\mathbb{R}^d$ that minimizes a "distance error" associated with a randomly placed point and the nearest point of the point process.

It is noteworthy for what follows that the quantizer and covering optimization problems have been reformulated as certain ground-state problems involving the "void" exclusion probability $E_V(r)$ Torquato (2010), which was defined in Section 2.3. For example, the quantizer problem minimizes the first moment of $E_V(r)$ or, equivalently, the second moment of the associated nearest-neighbor probability function $H_V(r)$ [cf. (28)]. Since the first moment of $E_V(r)$ is directly connected to the second moment $\langle\delta^2\rangle$ of the pore-size probability function (26) for a packing, then it is expected that $\langle\delta^2\rangle$ among packings of identical spheres at the same packing fraction is minimized by the BCC packing. All of these results suggest that the size of the largest *probe* sphere that can traverse the pore space of a packing in the infinite-volume limit at packing fraction $\phi_2$ is given by the BCC packing for $0 \le \phi_2 \le \phi_{\max}^{BCC}$, where $\phi_{\max}^{BCC} = \sqrt{3}\pi/8 = 0.68017\ldots$ is the maximum packing fraction for the BCC lattice consistent with the nonoverlap constraint. Note that the corresponding maximum packing fractions for SC and FCC lattices are $\phi_{\max}^{SC} = \pi/6 = 0.52359\ldots$ and $\phi_{\max}^{FCC} = \pi/\sqrt{18} = 0.74048\ldots$, respectively (Conway and Sloane, 1998).

#### 5.2.2. Disordered packings

We consider two different disordered hyperuniform packing models. The first is a maximally random jammed (MRJ) packing, which can be regarded to be the most random packing subject to strict jamming constraint (Torquato et al., 2000; Torquato, 2018b). This jamming condition implies that each sphere is in contact with its nearest neighbors such that there can be no "collective" particle motions that lead to unjamming, and they are stable against both uniform compression and shear deformations.

We also study "stealthy" packings, which are disordered and hyperuniform, and hence have spectral densities that satisfy the condition (17), where $K$ is the *exclusion sphere radius* in Fourier (reciprocal) space. Such packings have been created by decorating stealthy point configurations, generated via the so-called *collective-coordinate* optimization technique (Uche et al., 2004; Batten et al., 2008; Zhang et al., 2015), by spheres of radius $a$ such that spheres cannot overlap (Zhang et al., 2016b). Disordered stealthy point configurations generated by this optimization procedure are actually classical ground states of systems of particles interacting with bounded long-ranged pair potentials.

The control parameter is the exclusion sphere radius $K$. When $K$ is sufficiently small compared to the number of degrees of freedom, the ground states are disordered, stealthy and highly degenerate. However, when $K$ reaches a certain critical value, there is a phase transition to ordered ground states. It is noteworthy that at the highest value of $K$ in three dimensions, the ground state is uniquely the BCC lattice (Torquato et al., 2015). It is also remarkable that among all hyperuniform point configurations in three dimensions, the BCC lattice is believed to be the one that minimizes large-scale density fluctuations (Torquato and Stillinger, 2003; Zachary and Torquato, 2009). We will see that these properties of the BCC lattice impart singular fluid permeability properties to BCC packings.

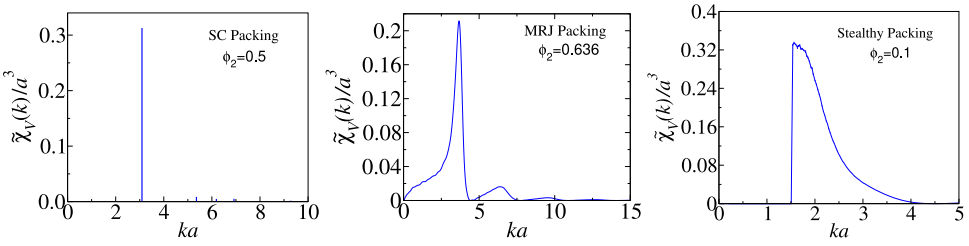


**Fig. 5.** Spectral densities for three different hyperuniform packing models: SC, MRJ and stealthy packings.

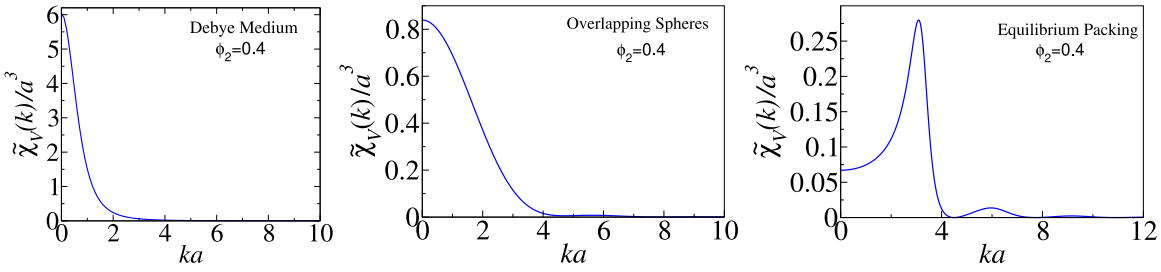


**Fig. 6.** Spectral densities for three different nonhyperuniform models at $\phi_2 = 0.4$: Debye random media, overlapping spheres and equilibrium packings.

### 5.3. Corresponding spectral densities and pore-Size statistics

We note that for any periodic point configuration of $N$ points within a fundamental cell of volume $v_F$ in three dimensions, the angular-averaged structure factor can be expressed as follows (Torquato, 2018a):

$$S(k) = \frac{8\pi^3}{v_F} \sum_{j=1}^{\infty} \frac{Z_j}{4\pi k^2} \delta(k - q_j), \tag{65}$$

where $Z_j$ is the number of points in reciprocal space at the Bragg-peak wavenumber $q_j$ and $\delta(r)$ is the radial Dirac delta function. The quantities $Z_j$ and $q_j$ are encoded in the *theta* series for the lattice (Conway and Sloane, 1998). Eq. (65) together with (19) yields the corresponding analytical expression for the spectral density of general crystal packing of identical spheres of radius $a$:

$$\tilde{\chi}_V(k) = \frac{3\pi\phi_2}{2\,a^3\,v_F}\,\tilde{m}^2(k;a) \sum_{j=1}^{\infty} \frac{Z_j}{k^2}\,\delta(k - q_j). \tag{66}$$

This expression clearly reveals that lattice packings are stealthy [cf. (17)] and hyperuniform. Since the envelope of $\tilde{m}^2(k;a)$ is a rapidly decaying function of $k$, the weights of the delta functions decrease as $k$ increases, as shown in Fig. 5 for the case of the simple cubic lattice with $\phi_2 = 1/2$. The spectral density for hyperuniform MRJ sphere packings at $\phi_2 = 0.636$, determined from large-scale computer simulations (Klatt and Torquato, 2016), as well as for a stealthy packing at $\phi_2 = 0.1$, are also shown in Fig. 5. The latter is obtained using theoretically derived approximation formulas for the structure factor for stealthy point configurations (Torquato et al., 2015), expression (19) and the numerically determined radii provided in Ref. Zhang et al. (2016b).

In Fig. 6, we compare the spectral densities for the aforementioned three nonhyperuniform models, each at $\phi_2 = 0.4$. The spectral density for Debye random media in any space dimension is given by

$$\tilde{\chi}_V(k) = \frac{\phi_1\phi_2\,c_d\,a^d}{[1 + (ka)^2]^{(d+1)/2}}, \tag{67}$$

where $c_d = 2^d\pi^{(d-1)/2}\Gamma((d+1)/2)$. The spectral density $\tilde{\chi}_V(k)$ for overlapping spheres is straightforwardly obtained by taking the Fourier transform of (60). For equilibrium hard spheres, the spectral density at packing fraction $\phi_2$ is obtained from Eq. (19) and the Percus-Yevick approximation (Torquato and Stell, 1985; Torquato, 2002a).

The exact pore-size probability function $F(\delta)$ for each of the three lattice packings is easily obtained from exact results for the exclusion probability $E_V(r)$ (Torquato, 2010) and then applying the mapping (27). Since a test sphere of radius $\delta_c$ and larger cannot be inserted in a lattice packing, $F(\delta)$ has compact support, i.e., $F(\delta) = 0$ for $\delta \geq \delta_c$. The pore-size function $F(\delta)$ for the MRJ packing has been determined from large-scale computer simulations in Refs. Donev et al. (2005) and Klatt and Torquato (2016) From recent theoretical and computer-simulation studies of the exclusion probability of stealthy systems (Torquato et al., 2015; Zhang et al., 2016a), we can extract the pore-size function $F(\delta)$ for disordered stealthy packings. It follows that since disordered stealthy point configurations have the property that $E_V(r)$ has compact support (Zhang et al., 2017; Ghosh and Lebowitz, 2018), an unusual behavior for a disordered system, the pore-size function $F(\delta)$ of a disordered stealth packing of identical spheres will also have compact support. Using accurate formulas for the exclusion probability $E_V(r)$ (Torquato et al., 1990), the pore-size function $F(\delta)$ has been determined for equilibrium hard spheres (Torquato, 2002a) using (27). In three dimensions, the pore-size probability for overlapping spheres is exactly given by Torquato (2002a)

$$F(\delta) = \frac{1}{\phi_1}\exp\left[-\eta(1 + \delta/a)^3\right]. \tag{68}$$

Note that (68)(has infinite support, which implies that the pore space possesses arbitrarily large "holes" in the infinite-volume limit. This characteristic of nonhyperuniform overlapping spheres applies as well to nonhyperuniform equilibrium packings (Torquato, 2002a), which has important implications for NMR time scales, as described in the next section. This is due to the fact the pore-size function $F(\delta)$ in each of these nonhyperuniform models has infinite support; It is noteworthy that the pore-size functions of Debye random media have yet to be determined.

It is useful to compare the pore-size function of stealthy hyperuniform packings to those of hyperuniform BCC packings and nonhyperuniform overlapping spheres. Fig. 7 provides such a comparison of $F(\delta)$ on a log scale at $\phi_2$. Not surprisingly, the two stealthy cases exhibit similar behaviors, i.e., $F(\delta)$ dropping precipitously as $\delta$ approaches its maximum values, which is in stark contrast to the very gradual drop of $F(\delta)$ with $\delta$ for the overlapping-spheres case.

## 6. Estimates of effective properties for hyperuniform and nonhyperuniform models

### 6.1. Formation factor

In Fig. 8, we compare the formation factor $\mathcal{F}$ as a function of $\phi_2$ for two hyperuniform systems, BCC and stealthy packings, and two nonhy-

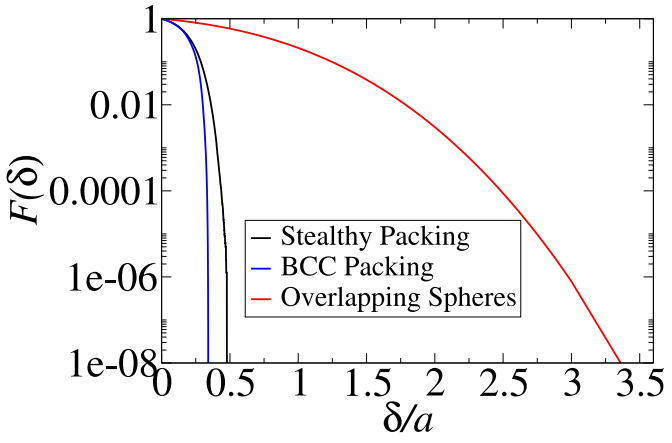


**Fig. 7.** Comparison of the pore-size probability $F(\delta)$ for the BCC packing, stealthy hyperuniform packing and overlapping spheres at $\phi_2 = 0.2$. The BCC and stealthy cases are obtained from the void exclusion probability functions $E_V(r)$ presented in Refs. Torquato (2010) and Zhang et al. (2016b) and then applying the mapping (27). The corresponding overlapping-spheres result is obtained from the analytical expression given in Ref. Torquato (2002a).

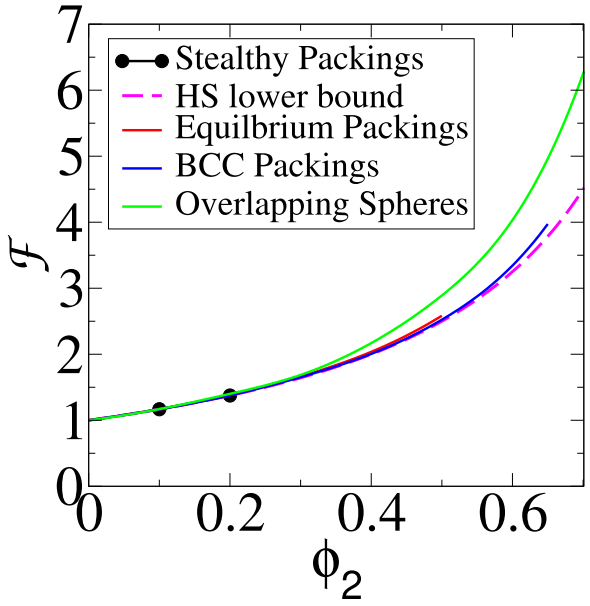


**Fig. 8.** Comparison of formation factor $\mathcal{F}$ as a function of $\phi_2$ for two hyperuniform systems (BCC and stealthy packings), and two nonhyperuniform systems (equilibrium hard-sphere packings and overlapping spheres). The optimal Hashin-Shtrikman lower bound is also shown.

peruniform systems, equilibrium hard-sphere packings and overlapping spheres. Such a comparison has heretofore not been presented. We also include the Hashin-Shtrikman lower bound to see how close these formation factors are to being extremal. Data for the BCC and stealthy packings are taken from numerical studies of the effective conductivity from Refs. McKenzie et al. (1978) and Zhang et al. (2016b), respectively. The formation factor for equilibrium hard sphere packings was determined from a highly accurate microstructure-dependent approximation formula (49) Torquato (1985) as well as computer-simulation data Kim and Torquato (1991) for the effective conductivity. Note that the formation factors for the stealthy packings are effectively optimal, i.e., they are the same as the Hashin-Shtrikman lower bound (Zhang et al., 2016b) to three significant figures and hence cannot be distinguished from one another on the scale of this figure. Not surprisingly, formation factors

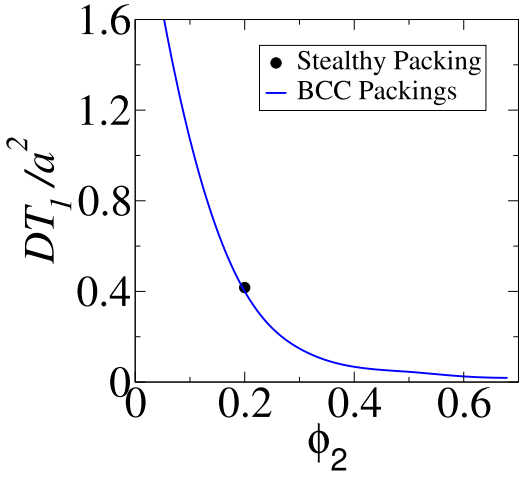


**Fig. 9.** Principal relaxation time $T_1$ versus $\phi_2$ for BCC and a stealthy packing in the pure diffusion-controlled limit. By contrast, both nonhyperuniform overlapping spheres and nonhyperuniform equilibrium packings have unbounded principal relaxation times, as discussed in the text.

for overlapping spheres deviate the most from the optimal lower bound and increasingly so as $\phi_2$ increases.

### 6.2. NMR time scales

Now we consider results for NMR time scales in the pure diffusion-controlled limit, i.e., infinite surface reaction ($\kappa = \infty$), implying perfect absorption at the trap-pore interface. Recently, the mean survival time $\tau$ and principal relaxation time $T_1$ have been computed for stealthy packings in which the particles are perfect absorbers (Zhang et al., 2016b). In the present work, we compare them, for the first time, to earlier corresponding results for BCC packings from a computer-simulation study of Torquato and Kim (1992). For brevity, it suffices here to report such a comparison for $T_1$; see Refs. Zhang et al. (2016b) and Torquato and Stillinger (2002) for results for the means survival time.

Fig. 9 shows a comparison of the principal relaxation time $T_1$ of a stealthy packing at $\phi_2 = 0.2$ to the corresponding result for a BCC packing. This figure also includes BCC results for other packing fractions. It is seen that the stealthy packing has a principal relaxation time that is very nearly equal to that of the BCC packing at $\phi_2 = 0.2$. This is expected, since both systems are not only hyperuniform but stealthy, and hence are characterized by appreciably diminished pore-size fluctuations, as noted in Section 5.3. In vivid contrast to these results is the fact that $T_1$ for both nonhyperuniform overlapping spheres and nonhyperuniform equilibrium packings become unbounded in the infinite-volume limit Torquato (1990), since the pore space possesses arbitrarily large "holes" in this limit, as discussed in Section 5.3.

### 6.3. Fluid permeability

#### 6.3.1. Two-point void bound

We utilize the two-point void bound (54) to infer how the permeabilities of hyperuniform porous media perform relative to those of nonhyperuniform ones. However, it may be difficult to evaluate numerically the integral in the direct-space formula (52) for the length scale $\ell_P$, since the integrand of (52) can be both positive and negative due positive and negative correlations that would be reflected in $\chi_V(r)$. It becomes especially nontrivial to compute if $\chi_V(r)$ slowly converges, as in the case of many hyperuniform media, where one must not only estimate $\chi_V(r)$ precisely but rely on a complex extrapolation technique known as $\alpha$ convergence (Torquato and Stillinger, 2003; Klatt and Torquato, 2018) (see also the Appendix for additional details).

**Table 1**
Two-point void upper bound on the dimensionless fluid permeability $k/a^2$ for various packings of identical spheres of radius $a$ at selected values of the packing fraction $\phi_2$. This includes hyperuniform packings (3 lattice packings and stealthy packings) and nonhyperuniform equilibrium packings. The MRJ packing has the unique packing fraction of $\phi_2 \approx 0.636$. 3D stealthy packings do not exist at $\phi_2 = 0.5$ and 0.636 (Zhang et al., 2016b). The maximum packing fraction for spheres arranged on a SC lattice is $\phi_2 = \pi/6 = 0.5235\ldots$. Equilibrium packings do not exist at $\phi_2 \approx 0.636$ (Torquato, 2002a; 2018b).

| | Dimensionless permeability $ka^2$ | | | | | |
|---|---|---|---|---|---|---|
| $\phi_2$ | SC | FCC | BCC | Stealthy | MRJ | Equilibrium |
| 0.1 | 0.9845 | 0.9519 | 0.9518 | 0.9970 | — | 1.7100 |
| 0.2 | 0.3230 | 0.3024 | 0.3023 | 0.3360 | — | 0.5486 |
| 0.5 | 0.04577 | 0.03461 | 0.03458 | — | | 0.1551 |
| 0.636 | — | 0.01424 | 0.01420 | — | 0.02047 | — |

**Table 2**
Two-point void upper bound on the dimensionless fluid permeability $ks^2$ for two nonhyperuniform models: overlapping spheres and Debye random media at selected values of the volume fraction $\phi_2$. The values of the specific surface $s$ of the former and latter are given by (61) and (64), respectively.

| | Dimensionless permeability $ks^2$ | |
|---|---|---|
| $\phi_2$ | Overlapping spheres | Debye random media |
| 0.1 | 0.1885 | 0.7776 |
| 0.2 | 0.2870 | 1.0923 |
| 0.3 | 0.3148 | 1.0976 |
| 0.4 | 0.2911 | 0.9216 |
| 0.5 | 0.2346 | 0.6667 |
| 0.6 | 0.1629 | 0.4096 |
| 0.7 | 0.0926 | 0.2016 |
| 0.8 | 0.03738 | 0.06827 |
| 0.9 | 0.006655 | 0.009600 |

Since it is crucial to capture accurately the long-range structural behavior of hyperuniform media [i.e., the tail of the autocovariance function $\chi_V(r)$], we derive here an alternative Fourier representation of the relevant length scale $\ell_P$ [cf. (52)] that arises in the bound (54). First, we recall Parseval's theorem for direct-space functions $f(\mathbf{r})$ and $g(\mathbf{r})$ with well-defined corresponding Fourier transforms $\tilde{f}(\mathbf{k})$ and $\tilde{g}(\mathbf{k})$ in three-dimensional Euclidean space:

$$\int_{\mathbb{R}^3} f(\mathbf{r})\, g(\mathbf{r})\, d\mathbf{r} = \frac{1}{(2\pi)^3} \int_{\mathbb{R}^3} \tilde{f}(\mathbf{k})\, \tilde{g}(\mathbf{k})\, d\mathbf{k}. \tag{69}$$

Now we let $f(\mathbf{r}) = 1/(4\pi r)$ and $g(\mathbf{r}) = \chi_V(r)$ and recognize that the Fourier transform of $f(\mathbf{r})$ exists in the sense of distributions, i.e., $\tilde{f}(\mathbf{k}) = k^{-2}$. Thus, we find the alternative Fourier form of the length scale:

$$\ell_P^2 = \frac{1}{2\pi^2} \int_0^\infty \tilde{\chi}_V(k) dk. \tag{70}$$

The analogous Fourier representation of the interfacial surface upper bound on $k$ is provided in the Appendix.

Formula (70) has great advantages over the direct-space representation (52). First, the integrand of (70) is always nonnegative and hence not subject to the aforementioned to the precision issues in evaluating (52), where the medium is hyperuniform or not. Another advantage of the Fourier representation (70) occurs when the autocovariance function $\chi_V(r)$ oscillates and slowly decays to zero, such as in crystal (periodic) packings. For a crystal packing of identical spheres of radius $a$, combination of (19), (65) and (70) leads to the following expression for the length scale $\ell_P$:

$$\ell_P^2 = \frac{\phi_2}{v_F v_1(a)} \sum_{j=1}^{\infty} \frac{Z_j}{q_j^2}\, \tilde{m}^2(q_j; a). \tag{71}$$

Moreover, we see that truncation of the infinite series bounds the exact result from below, since each term in the series (71) is positive.

In summary, the new formula (70) conveniently captures the long-range correlations without a complex extrapolation required to compute (52) accurately and hence more precise estimates can be obtained with greater ease. It is quite versatile and easily applied to other models, including polydisperse sphere packings, for example.

We employ the spectral densities of various packings of identical spheres of radius $a$ described in Section 5.3 to compute the corresponding void bound on $k$ using formula (70) for $\ell_P$. Specifically, the void bound is calculated for the hyperuniform SC, FCC and BCC lattice packings, disordered stealthy packings and MRJ packing as well as nonhyperuniform equilibrium packings at selected values of the packing fraction $\phi_2$. These results are tabulated in Table 1 where the fluid permeability is scaled by $a^2$, the natural choice for nonoverlapping spheres of radius $a$. Importantly, while the void bound is not very tight, it does provide the proper ranking for the lattice packings for which we know the permeabilities accurately (Sangani and Acrivos, 1982), namely, at fixed $\phi_2$, a SC packing has slightly higher value of $k$ than a FCC packing, which in turn is slightly higher than the permeability of a BCC packing. We see that the stealthy hyperuniform packings have permeabilities that are slightly greater those of the SC packing, but much smaller than the corresponding values for the nonhyperuniform equilibrium packing. Note also the permeability of the hyperuniform MRJ packing at $\phi_2 = 0.636$ [which is in very good agreement with the numerical result reported in Ref. Klatt and Torquato (2018) using the direct-space formula (52)] is not appreciably larger than the corresponding values for the FCC and BCC packings at this packing fraction. Generally speaking, relative to nonhyperuniform porous media, hyperuniform ones are expected to have velocity fields that are more uniform throughout the pore space. Indeed, a recent microfluidics study in two dimensions confirms this conclusion (Ding et al., 2018). Moreover, stealthy hyperuniform packings, which include all of the lattice packings and disordered ones, cannot tolerate large "holes" for transport, and hence in each of these cases, the velocity field over the pore space is highly *delocalized* and the entire pore space is more uniformly dynamically connected. Thus, one expects the fluid permeability to be lower in all of the stealthy cases relative to the nonhyperuniform equlibrium instances in which the velocity field is more localized over the pore space due greater variability in the geometry of the pore "channels". The degree of delocalization of the velocity field in the case of hyperuniform porous media can be rigorously quantified by appealing to the generalization of the hyperuniformity concept to vector fields (Torquato, 2016b).

To get a visual sense of the distinctions between the pore space in hyperuniform versus nonhyperuniform porous media, we *dilate* the solid-phase region radially in equilibrium, MRJ and disordered stealthy packings so that the resulting pore space has a porosity of 1%. It is important to recall that while the MRJ packing is hyperuniform, it is not stealthy. The initial packing fractions are $\phi_2 = 0.25$, $\phi_2 = 0.2$ and $\phi_2 = 0.636$ for the equilibrium, MRJ and stealthy disordered packings, respectively. The resulting pore spaces are depicted in Fig. 10. The large variability in the size and shapes of the resultant pore regions in the nonhyperuniform equilibrium case relative to those in the hyperuniform instances is readily apparent. Moreover, the spatial distribution of the MRJ pore regions are less "uniform" than those of the disordered stealthy packing.

We also compute the two-point void bound for overlapping spheres and Debye random media, each of which depart appreciably from hyperuniformity. In order to compare these two distinctly different models, we utilize the square of the specific surface $s^2$ to scale the fluid permeability. These results are tabulated in Table 2. It is noteworthy that the upper bound on the scaled permeability for Debye random media is generally substantially larger than that for overlapping spheres at the same value of $\phi_2$. This strongly suggests that Debye random media are characterized by substantially larger pores (larger flow "channels") than those in the overlapping-sphere model. Indeed, this is quantitatively corroborated by the fact that the autocovariance function of Debye random

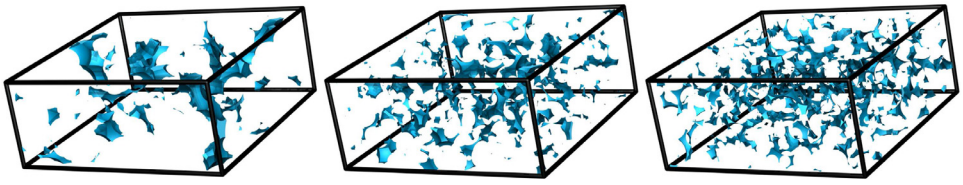

**Fig. 10.** Void space after applying a dilation operation to three different sphere packings: A nonhyperuniform equilibrium packing (left panel), a hyperuniform MRJ packing (middle panel) and a disordered stealthy packing (right panel). Movies showing these structures as they rotate in three-dimensional space are provided in the Supplementary Material.

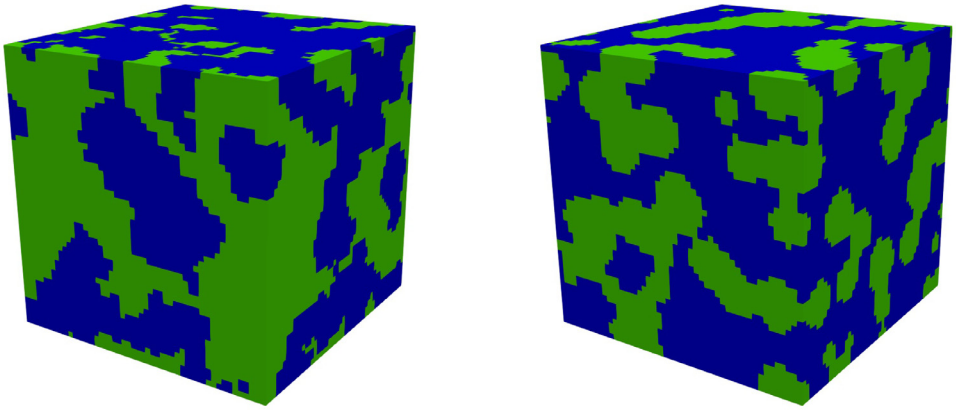

**Fig. 11.** Left panel: 3D construction of a digitized two-phase medium consisting of $51 \times 51 \times 51$ voxels that corresponds to a Debye random medium at $\phi_1 = \phi_2 = 1/2$ with an autocovariance function given by (62) with $a = 5$ in units of a voxels side length. Right panel: 3D realization of digitized system of overlapping spheres at the same resolution, system size, porosity and specific surface.

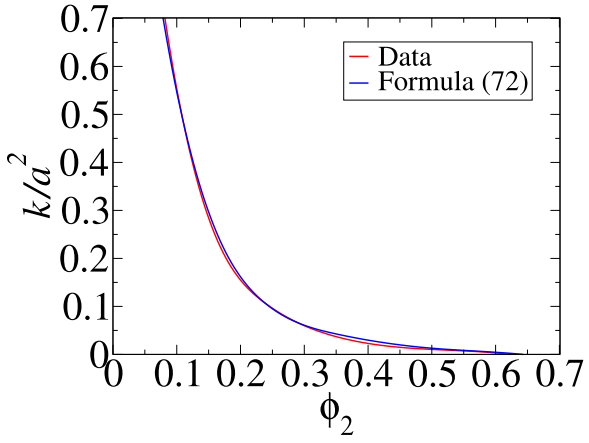


**Fig. 12.** Comparison of computer-simulation data for the fluid permeability of BCC packings as a function of $\phi_2$ to the predictions of formula (72).

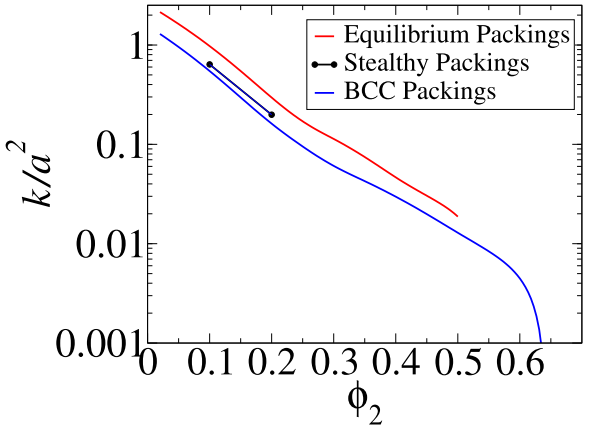


**Fig. 13.** Estimates of the dimensionless fluid permeability $k/a^2$ as a function of $\phi_2$ predicted by formula (72) for the disordered stealthy, equilibrium, and BCC packings.

media has infinite support [cf. (62], while that of overlapping spheres has compact support [cf. (60)]. As noted in Section 5.3, the actual pore-size function (68) of overlapping spheres has infinite support, the pore space possesses arbitrarily large 'holes" in the infinite-volume limit.

To verify whether this conclusion about the pore statistics of Debye random media can be inferred from the void bound, we have applied the Yeong and Torquato (1998a) stochastic optimization construction technique to generate a digitized 3D Debye random medium with $\phi_2 = 1/2$ (in a cube under periodic boundary conditions) in order to visualize it. Such a digitized realization, in which the two phases are statistically identical, is shown in Fig. 11. We also directly generated a corresponding digitized realization of overlapping spheres by randomly placing spheres in a cubic box under periodic boundary conditions at the same porosity, specific surface $s$ and resolution. It is clear that each phase in the Debye random medium is characterized by large clusters and pore sizes that are appreciably larger than those of its overlapping-sphere counterpart. This speaks to the utility of the two-point void bound to infer nontrivial microstructural information about the porous medium.

### 6.3.2. *New estimate of the fluid permeability*

While the two-point void bound (54) is able to capture the proper trends of how the permeability changes as the microstructures varies, it is not capable of providing sharp estimates of $k$. Let us assume there exists a class of porous media in which the inequality (53) on $T_1$ in the diffusion-controlled limit and the inequality (59) on $\mathcal{L}^2$ can be treated as equalities. Then, using the exact result (47), we obtain the following approximation for the fluid permeability:

$$k \approx \frac{\langle \delta^2 \rangle}{\mathcal{F}}, \tag{72}$$

which implies that the exact length scale $\mathcal{L}$ that appears in the exact relation (47) for the permeability is given by

$$\mathcal{L}^2 \approx \langle \delta^2 \rangle. \tag{73}$$

To test the validity of formula (72), we compare in Fig. 12 numerical data for the fluid permeability of BCC packings obtained by Sangani and Acrivos (1982) to the approximation formula (72). We see that formula (72) provides an excellent approximation of the simulation data of the fluid permeability. Thus, formula (72) should provide relatively accurate predictions of the permeability for microstructures in

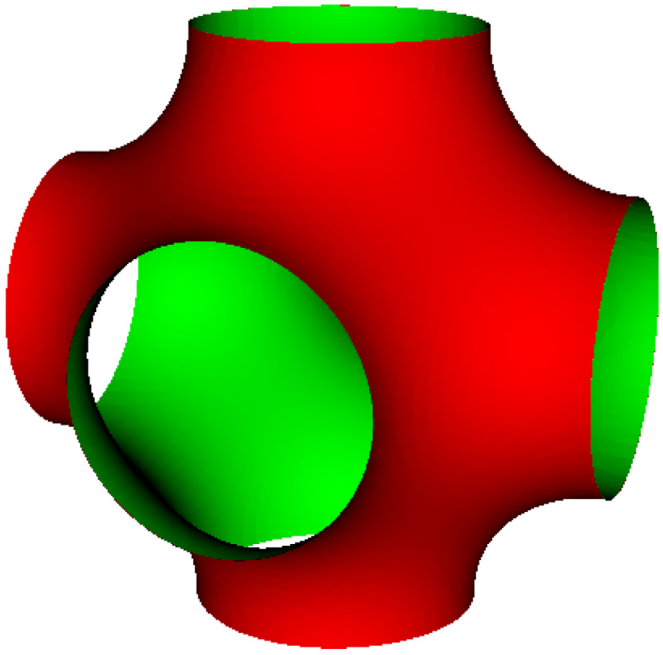

**Fig. 14.** Fundamental cell (smallest periodic repeat unit) showing the interface of the Schwartz *P* minimal surface, which was conjectured by Jung and Torquato Jung and Torquato (2005) to maximize the fluid permeability at porosity $\phi_1 = 1/2$ under the constraints described in the text.

which the pore space is well connected, including equilibrium packings, MRJ packings and lattice packings in which the spheres are not necessarily monodisperse. We compare the predictions of formula (72) for stealthy, equilibrium and BCC packings in Fig. 13. Formula (72) for equilibrium sphere packings was computed using previous results for the effective conductivity (Torquato, 1985; Kim and Torquato, 1991) and $\langle \delta^2 \rangle$ (Torquato and Avellaneda, 1991). Note that the permeability estimates for stealthy packings are substantially closer to those for the BCC packings, which is fully consistent with inferences we drew from the behavior of the void bound.

## 7. Conclusions and discussion

We have investigated and applied rigorous microstructure-property relations to estimate effective transport characteristics of hyperuniform and nonhyperuniform models of fluid-saturated porous media, including the formation factor $F$, mean survival time $\tau$, principal NMR (diffusion) relaxation time $T_1$, principal viscous relaxation time $\Theta_1$, and fluid permeability $k$. Among other results, we derived a Fourier representation of the classic two-point upper bound on the fluid permeability that depends on the spectral density to infer how the permeabilities of hyperuniform porous media perform relative to those of nonhyperuniform ones. We found that the velocity fields in nonhyperuniform porous media are generally much more localized over the pore space compared to those in their hyperuniform counterparts in which the velocity fields are more uniform throughout the pore space. The fluid permeability is expected to be lower in all of the stealthy hyperuniform cases relative to the nonhyperuniform equlibrium instances due to their greater variability in the geometry of the pore "channels". Our analysis of the void bounds on the permeability for the SC, FCC and BCC lattice packings provides the first quantitative explanation for why the BCC lattice packing minimizes the permeability among these crystal structures at fixed $\phi_2$. This bound also enabled us to correctly infer that nonhyperuniform Debye random media should be characterized by substantially large pore regions, which was verified by constructing a realization of such a porous medium. Rigorous bounds on individual effective properties as well as cross-property relations suggested a new approximate formula (72) for the permeability given in terms of the formation factor $F$ and the second moment $\langle \delta^2 \rangle$ of the pore-size probability density, the latter of which can be easily extracted from 3D digitized images of real porous media (Coker et al., 1996). Formula (72) provides reasonably accurate permeability predictions of the class of hyperuniform and nonhyperuniform porous media in which the pore space is well connected. The permeability estimates for disordered stealthy hyperuniform packings were shown to be substantially closer to those for the BCC packings, which is fully consistent with inferences we drew from the behavior of the void bound. These comparative studies have shed new light on the microstructural characteristics that determine the transport properties of general porous media.

An outstanding problem for future research is the direct Stokes-flow simulations of models of disordered hyperuniform porous media to determine their fluid permeabilities. Part of such a program could include the creation of disordered hyperuniform pore network models of porous media at arbitrary porosities and the computation of their transport properties. Another interesting problem for future research is the determination of the pore-size functions of Debye random media. Since there is a degeneracy of microstructures with an autocovariance function specified by (62) but with different higher-order statistics, the pore-size function of Debye random media will depend on the stochastic rules to construct them.

We note that our findings also have implications for the design of disordered hyperuniform porous materials with desirable transport properties. Specifically, such 3D porous media can be fabricated using 3D additive manufacturing techniques (Kim and Torquato, 2019b).

We close this section with simple observations about an outstanding optimization problem posed by Jung and Torquato (Jung and Torquato, 2005) in the light of the hyperuniformity concept. They asked what microstructure(s) under periodic boundary conditions in a cubic fundamental (unit) cell of unit side length maximizes the isotropic fluid permeability $k$ at some porosity? They focused on the case $\phi_1 = 1/2$ and computed the permeabilities of a variety of different candidate structures, including triply periodic minimal surfaces, due to their optimality for other physical properties (Torquato et al., 2002; Torquato and Donev, 2004). They conjectured that the triply periodic two-phase bicontinuous porous medium with an interface that is the Schwartz primitive (P) minimal surface (see Fig. 14) maximizes the isotropic fluid permeability. This surmise follows from another conjecture that they put forth and supported by calculations Torquato et al. (2002) and analysis (Jung et al., 2007), namely, the Schwartz P structure has the minimal specific surface under the aforementioned constraints. This is still a fascinating open question and is a type of isoperimetric problem in the same spirit as Kelvin's famous conjecture about foams (Weaire and Phelan, 1994). Finally, we observe that the conjectured extremal Schwartz P structure for the fluid permeability is stealthy and hyperuniform.

## Declaration of interests

The authors declare that they have no known competing financial interests or personal relationships that could have appeared to influence the work reported in this paper.

## Acknowledgement

I am deeply grateful to Michael Klatt for the creation of the images in Fig. 10 and the right panel of Fig. 11, Zheng Ma for the creation of the image in the left panel of Fig. 11, and Jaeuk Kim for his assistance in creating the stealthy-packing plot of Fig. 5. I thank all three of them for their very helpful remarks on the manuscript. This work was supported by the Air Force Office of Scientific Research Program on Mechanics of Multifunctional Materials and Microsystems under award No. FA9550-18-1-0514.

## Appendix A. Two-Point Interfacial Surface Upper Bound

The two-point *surface* correlation functions, such as the surface-surface correlation function $F_{ss}(r)$, and surface-void correlation function $F_{sv}(r)$ (Torquato, 2002a) are crucial in determining transport properties of porous media when the interface plays a major role, such as the mean survival time and fluid permeability (Doi, 1976; Rubinstein and Torquato, 1988; 1989). Until recently, the difficulty of sampling surface correlation functions of porous media has been a stumbling block in their widespread use. It has recently been shown that one can reduce the computational complexity of brute-force sampling, without sacrificing accuracy, by extracting the necessary interfacial information from a cut of a statistically homogeneous and isotropic $d$-dimensional medium (in continuous and discrete spaces) with an infinitely long line (Ma and Torquato, 2018).

The two-point "interfacial-surface" upper bound on the isotropic fluid permeability (Doi, 1976; Rubinstein and Torquato, 1989) is given by

$$k \leq \frac{2}{3}\ell_S^2, \tag{A.1}$$

where

$$\ell_S^2 = \int_0^\infty \left[\frac{\phi_1^2}{s^2}F_{ss}(r) - \frac{2\phi_1}{s}F_{sv}(r) + F_{vv}(r)\right] r dr, \tag{A.2}$$

where $F_{vv}(r) \equiv S_2^{(1)}(r)$. This bound is generally sharper than the void bound (54), which involves $S_2^{(1)}(r)$ alone (Doi, 1976; Rubinstein and Torquato, 1989). Analogously to the void bound, the direct-space formula (A.2) is numerically very challenging. Klatt and Torquato (2018) addressed these challenges to compute the interfacial surface bound for disordered monodisperse sphere packings, including equilibrium and MRJ packings, by deriving the corresponding analytic formulas for finite samples.

However, as in the case of the void bound, it is substantially easier numerically to employ a Fourier-based formula, especially for hyperuniform media. To derive the Fourier representation of the length scale $\ell_S$, we first define the relevant autocovariance functions for statistically homogeneous media. Specifically,

$$\chi_S(\mathbf{r}) = F_{ss}(\mathbf{r}) - s^2, \tag{A.3}$$

is the autocovariance function associated with $F_{ss}(r)$, and

$$\chi_{SV}(\mathbf{r}) = F_{sv}(\mathbf{r}) - s\phi_1, \tag{A.4}$$

is the cross-covariance function associated with $F_{sv}(\mathbf{r})$. The corresponding spectral densities $\tilde{\chi}_S(\mathbf{k})$ and $\tilde{\chi}_{SV}(\mathbf{k})$ are obtained by taking the Fourier transforms of $\chi_S(\mathbf{r})$ and $\chi_{SV}(\mathbf{r})$, respectively. Application of Parseval's theorem in the integral (A.2), yields its Fourier representation:

$$\ell_S^2 = \ell_P^2 + \frac{1}{2\pi^2}\int_0^\infty \left[\frac{\phi_1^2}{s^2}\tilde{\chi}_S(k) - \frac{2\phi_1}{s}\tilde{\chi}_{SV}(k)\right] dk, \tag{A.5}$$

where $\ell_P^2$ is given by (52). The same applies to the analogous two-point interfacial surface bound on the mean survival time (Doi, 1976; Rubinstein and Torquato, 1988).

## Supplementary material

Supplementary material associated with this article can be found, in the online version, at doi:10.1016/j.advwatres.2020.103565.

## References


Sen, A.K., Torquato, S., 1989. Effective conductivity of anisotropic two-phase composite media. Phys. Rev. B 39, 4504–4515.

Sen, P.N., Hürlimann, M.D., 1994. Analysis of nuclear magnetic resonance spin echoes using simple structure factors. J. Chem. Phys. 101, 5423–5430.

Aramideh, S., Vlachos, P.P., Ardekani, A.M., 2018. Pore-scale statistics of flow and transport through porous media. Phys. Rev. E 98, 013104.

Ashcroft, N.W., Mermin, D.N., 1976. Solid State Physics. Thomson Learning, Toronto.

Avellaneda, M., Torquato, S., 1991. Rigorous link between fluid permeability, electrical conductivity, and relaxation times for transport in porous media. Phys. Fluids A 3, 2529–2540.

Batten, R.D., Stillinger, F.H., Torquato, S., 2008. Classical disordered ground states: super-ideal gases, and stealth and equi-luminous materials. J. Appl. Phys. 104, 33504.

Beran, M., 1965. Use of the variational approach to determine bounds for the effective permittivity in random media. Nuovo Cimento 38, 771–782.

Bergman, D.J., Dunn, K.J., 1994. Theory of diffusion in a porous medium with applications to pulsed-field-gradient nmr. Phys. Rev. B 50, 9153.

Berryman, J.G., Milton, G.W., 1985. Normalization constraint for variational bounds on fluid permeability. J. Chem. Phys. 83, 754–760.

Bijeljic, B., Blunt, M.J., 2006. Pore-scale modeling and continuous time random walk analysis of dispersion in porous media. Water Resour. Res. 42, W01202. https://doi.org/10.1029/2005WR004578.

Blunt, M.J., Bijeljic, B., Dong, H., Gharbi, O., Iglauer, S., Mostaghimi, P., Paluszny, A., Pentland, C., 2013. Pore-scale imaging and modelling. Adv. Water Resour. 51, 197–216.

Brauchart, J.S., Grabner, P.J., Kusner, W., 2019. Hyperuniform point sets on the sphere: deterministic aspects. Construct. Approx. 50, 45–61.

Brown, W.F., 1955. Solid mixture permittivities. J. Chem. Phys. 23, 1514–1517.

Chaikin, P.M., Lubensky, T.C., 1995. Principles of condensed matter physics. Cambridge University Press, New York.

Chen, D., Torquato, S., 2018. Designing disordered hyperuniform two-phase materials with novel physical properties. Acta Mater. 142, 152–161.

Coker, D.A., Torquato, S., Dunsmuir, J.H., 1996. Morphology and physical properties of fontainebleau sandstone via a tomographic analysis. J. Geophys. Res. 101, 17497–17506.

Conway, J.H., Sloane, N.J.A., 1998. Sphere Packings. Lattices and Groups. Springer-Verlag, New York.

Dandekar, A.Y., 2013. Petroleum Reservoir Rock and Fluid Properties. CRC press.

Debye, P., Anderson, H.R., Brumberger, H., 1957. Scattering by an inhomogeneous solid. II. the correlation function and its applications. J. Appl. Phys. 28, 679–683.

Debye, P., Bueche, A.M., 1949. Scattering by an inhomogeneous solid. J. Appl. Phys. 20, 518–525.

Ding, Z., Zheng, Y., Xu, Y., Jiao, Y., Li, W., 2018. Hyperuniform flow fields resulting from hyperuniform configurations of circular disks. Phys. Rev. E 98, 063101.

Doi, M., 1976. A new variational approach to the diffusion and the flow problem in porous media. J. Phys. Soc. Japan 40, 567–572.

Donev, A., Stillinger, F.H., Torquato, S., 2005. Unexpected density fluctuations in disordered jammed hard-sphere packings. Phys. Rev. Lett. 95, 090604.

Elam, W.T., Kerstein, A.R., Rehr, J.J., 1984. Critical properties of the void percolation problem for spheres. Phys. Rev. Lett. 52, 1516–1519.

Florescu, M., Torquato, S., Steinhardt, P.J., 2009. Designer disordered materials with large complete photonic band gaps. Proc. Nat. Acad. Sci. 106, 20658–20663.

Froufe-Pérez, L.S., Engel, M., Sáenz, J.J., Scheffold, F., 2017. Transport phase diagram and anderson localization in hyperuniform disordered photonic materials. Proc. Nat. Acad. Sci. 114, 9570–9574.

Ghosh, S., Lebowitz, J.L., 2018. Generalized stealthy hyperuniform processes: maximal rigidity and the bounded holes conjecture. Commun. Math. Phys. 363, 97–110.

Gillman, A., Amadio, G., Matouš, K., Jackson, T.L., 2015. Third-order thermo-mechanical properties for packs of Platonic solids using statistical micromechanics. Proc. R. Soc. Lond. A 471. 20150060.

Gillman, A., Matouš, K., 2014. Third-order model of thermal conductivity for random polydisperse particulate materials using well-resolved statistical descriptions from tomography. Phys. Lett. A 378, 3070–3073.

Gorsky, S., Britton, W.A., Chen, Y., Montaner, J., Lenef, A., Raukas, M., Negro, L.D., 2019. Engineered hyperuniformity for directional light extraction. APL Photonic. 4, 110801.

Hansen, J.P., McDonald, I.R., 1986. Theory of Simple Liquids. Academic Press, New York.

Hashin, Z., Shtrikman, S., 1962. A variational approach to the theory of the effective magnetic permeability of multiphase materials. J. Appl. Phys. 33, 3125–3131.

Hashin, Z., Shtrikman, S., 1963. A variational approach to the elastic behavior of multiphase materials. J. Mech. Phys. Solids 4, 286–295.

Hexner, D., Levine, D., 2015. Hyperuniformity of critical absorbing states. Phys. Rev. Lett. 114, 110602.

Jiao, Y., Lau, T., Hatzikirou, H., Meyer-Hermann, M., Corbo, J.C., Torquato, S., 2014. Avian photoreceptor patterns represent a disordered hyperuniform solution to a multiscale packing problem. Phys. Rev. E 89, 022721.

Jiao, Y., Stillinger, F.H., Torquato, S., 2007. Modeling heterogeneous materials via two–point correlation functions: basic principles. Phys. Rev. E 76, 31110.

Jiao, Y., Stillinger, F.H., Torquato, S., 2009. A superior descriptor of random textures and its predictive capacity. Proc. Nat. Acad. Sci. 106, 17634–17639.

Johnson, D.L., Koplik, J., Schwartz, L.M., 1986. New pore-size parameter characterizing transport in porous media. Phys. Rev. Lett. 57, 2564–2567.

Jung, Y., Chu, K.T., Torquato, S., 2007. A variational level set approach for surface area minimization of triply periodic media. J. Comput. Phys. 223, 711–730.

Jung, Y., Torquato, S., 2005. Fluid permeabilities of triply periodic minimal surfaces. Phys. Rev. E 92, 255505.

Kim, I.C., Torquato, S., 1991. Effective conductivity of suspensions of hard spheres by brownian motion simulation. J. Appl. Phys. 69, 2280–2289.

Kim, J., Torquato, S., 2019. Methodology to construct large realizations of perfectly hyperuniform disordered packings. Phys. Rev. E 99, 052141.

Kim, J., Torquato, S., 2019. New tessellation-based procedure to design perfectly hyperuniform disordered dispersions for materials discovery. Acta Mater. 168, 143–151.

Kinney, J.H., Nichols, M.C., 1992. X-Ray tomographic (XTM) microscopy using synchrotron radiation. Ann. Rev. Mater. Sci. 22, 121–152.

Klatt, M.A., Lovrić, J., Chen, D., Kapfer, S.C., Schaller, F.M., Schönhöfer, P.W.A., Gardiner, B.S., Smith, A.-S., Schröder-Turk, G.E., Torquato, S., 2019. Universal hidden order in amorphous cellular geometries. Nature Comm. 10, 811.

Klatt, M.A., Torquato, S., 2016. Characterization of maximally random jammed sphere packings. II. correlation functions and density fluctuations. Phys. Rev. E 94, 22152.

Klatt, M.A., Torquato, S., 2018. Characterization of maximally random jammed sphere packings. III. transport and electromagnetic properties via correlation functions. Phys. Rev. E 97, 12118.

Leseur, O., Pierrat, R., Carminati, R., 2016. High-density hyperuniform materials can be transparent. Optica 3, 763–767.

Lomba, E., Weis, J.-J., Torquato, S., 2018. Disordered multihyperuniformity derived from binary plasmas. Phys. Rev. E 97, 010102(R).

Lu, B.L., Torquato, S., 1990. Local volume fraction fluctuations in heterogeneous media. J. Chem. Phys. 93, 3452–3459.

Ma, Z., Torquato, S., 2018. Precise algorithms to compute surface correlation functions of two-phase heterogeneous media and their applications. Phys. Rev. E 98, 013307.

Man, W., Florescu, M., Williamson, E.P., He, Y., Hashemizad, S.R., Leung, B.Y.C., Liner, D.R., Torquato, S., Chaikin, P.M., Steinhardt, P.J., 2013. Isotropic band gaps and freeform waveguides observed in hyperuniform disordered photonic solids. Proc. Nat. Acad. Sci. 110, 15886–15891.

Martys, N., Torquato, S., Bentz, D.P., 1994. Universal scaling of fluid permeability for sphere packings. Phys. Rev. E 50, 403–408.

Mayer, A., Balasubramanian, V., Mora, T., Walczak, A.M., 2015. How a well-adapted immune system is organized. Proc. Nat. Acad. Sci. 112, 5950–5955.

McKenzie, D.R., McPhedran, R.C., Derrick, G.H., 1978. The conductivity of lattices of spheres. II. the body centered and face centered cubic lattices. Proc. R. Soc. Lond. A 362, 211–232.

Milton, G.W., 1987. Multicomponent composites, electrical networks and new types of continued fractions. I and II, Commun. Math. Phys. 111, 281–372.

Milton, G.W., 2002. The Theory of Composites. Cambridge University Press, Cambridge, England.

Mitra, P.P., Sen, P.N., Schwartz, L.M., 1993. Short-time behavior of the diffusion coefficient as a geometrical probe of porous media. Phys. Rev. B 47, 8565–8574.

Mitra, P.P., Sen, P.N., Schwartz, L.M., Doussal, P.L., 1992. Diffusion propagator as a probe of the structure of porous media. Phys. Rev. Lett. 68, 3555.

Nguyen, M.-T., Monchiet, V., Bonnet, G., To, Q.D., 2016. Conductivity estimates of spherical-particle suspensions based on triplet structure factors. Phys. Rev. E 93. 022105.

Øren, P.E., Antonsen, F., Rueslåtten, H.G., Bakke, S., 2002. Numerical simulations of NMR responses for improved interpretations of nmr measurements in reservoir rocks. In: SPE Annual Technical Conference and Exhibition, Society of Petroleum Engineers.

Prager, S., 1961. Viscous flow through porous media. Phys. Fluids 4, 1477–1482.

Prager, S., 1963. Interphase transfer in stationary two-phase media. Chem. Eng. Sci. 18, 227–231.

Quintanilla, J., Torquato, S., 1997. Local volume fraction fluctuations in random media. J. Chem. Phys. 106, 2741–2751.

Quintard, M., Whitaker, S., 1994. Transport in ordered and disordered porous media i: the cellular average and the use of weighting functions. Transp. Porous Media 14, 163–177.

Quintard, M., Whitaker, S., 1994. Transport in ordered and disordered porous media II: generalized volume averaging. Transp. Porous Media 14, 179–206.

Rintoul, M.D., 2000. Precise determination of the void percolation threshold for two distributions of overlapping spheres. Phys. Rev. E 62, 68–72.

Rintoul, M.D., Torquato, S., 1997. Precise determination of the critical threshold and exponents in a three-dimensional continuum percolation model. J. Phys. A 30, L585–L592.

Robinson, D.A., Friedman, S.P., 2005. Electrical conductivity and dielectric permittivity of sphere packings: measurements and modelling of cubic lattices, randomly packed monosize spheres and multi-size mixtures. Phys. A 358, 447–465.

Rubinstein, J., Torquato, S., 1988. Diffusion-controlled reactions: mathematical formulation, variational principles, and rigorous bounds. J. Chem. Phys. 88, 6372–6380.

Rubinstein, J., Torquato, S., 1989. Flow in random porous media: mathematical formulation, variational principles, and rigorous bounds. J. Fluid Mech. 206, 25–46.

Sahimi, M., 2003. Heterogeneous Materials I: Linear Transport and Optical Properties. Springer-Verlag, New York.

Sangani, A.S., Acrivos, A., 1982. Slow flow through a periodic array of spheres. Int. J. Multiphase Flow 8, 343–360.

Scheidegger, A.E., 1974. The Physics of Flow Through Porous Media. University of Toronto Press, Toronto, Canada.

Stoyan, D., Kendall, W.S., Mecke, J., 1995. Stochastic Geometry and Its Applications, 2nd Edition. Wiley, New York.

Tahmasebi, P., 2018. Accurate modeling and evaluation of microstructures in complex materials. Phys. Rev. E 97, 023307.

Tahmasebi, P., Sahimi, M., 2013. Cross-correlation function for accurate reconstruction of heterogeneous media. Phys. Rev. Lett. 110, 078002.

Thien, Q.L., McDermott, D., Reichhardt, C.J.O., Reichhardt, C., 2017. Enhanced pinning for vortices in hyperuniform substrates and emergent hyperuniform vortex states. Phys. Rev. B 96, 094516.

Thompson, A.H., Katz, A.J., Krohn, C.E., 1987. The microgeometry and transport properties of sedimentary rock. Adv. Phys. 36, 625–694.

Todd, D.K., Mays, L.W., 2004. Groundwater Hydrology. Wiley, New York.

Torquato, S., 1985. Effective electrical conductivity of two-phase disordered composite media. J. Appl. Phys. 58, 3790–3797.

Torquato, S., 1990. Relationship between permeability and diffusion-controlled trapping constant of porous media. Phys. Rev. Lett. 64, 2644–2646.

Torquato, S., 1997. Exact expression for the effective elastic tensor of disordered composites. Phys. Rev. Lett. 79, 681–684.

Torquato, S., 2002. Random Heterogeneous Materials: Microstructure and Macroscopic Properties. Springer-Verlag, New York.

Torquato, S., 2002. Statistical description of microstructures. Ann. Rev. Mater. Res. 32, 77–111.

Torquato, S., 2010. Reformulation of the covering and quantizer problems as ground states of interacting particles. Phys. Rev. E 82, 056109.

Torquato, S., 2016. Disordered hyperuniform heterogeneous materials. J. Phys. 28, 414012.

Torquato, S., 2016. Hyperuniformity and its generalizations. Phys. Rev. E 94. 022122

Torquato, S., 2018. Hyperuniform states of matter. Phys. Rep. 745, 1–95.

Torquato, S., 2018. Perspective: basic understanding of condensed phases of matter via packing models. J. Chem. Phys. 149, 20901.

Torquato, S., Avellaneda, M., 1991. Diffusion and reaction in heterogeneous media: pore size distribution, relaxation times, and mean survival time. J. Chem. Phys. 95, 6477–6489.

Torquato, S., Chen, D., 2018. Multifunctional hyperuniform cellular networks: optimality, anisotropy and disorder. Multifunct. Mater. 1, 015001.

Torquato, S., Donev, A., 2004. Minimal surfaces and multifunctionality. Proc. R. Soc. Lond. A 460, 1849–1856.

Torquato, S., Hyun, S., Donev, A., 2002. Multifunctional composites: optimizing microstructures for simultaneous transport of heat and electricity. Phys. Rev. Lett. 89, 266601.

Torquato, S., Kim, I.C., 1992. Cross-property relations for momentum and diffusional transport in porous media. J. Appl. Phys. 72, 2612–2619.

Torquato, S., Lu, B., Rubinstein, J., 1990. Nearest-neighbor distribution functions in many-body sytems. Phys. Rev. A 41, 2059–2075.

Torquato, S., Pham, D.C., 2004. Optimal bounds on the trapping constant and permeability of porous media. Phys. Rev. Lett. 92, 255505.

Torquato, S., Rubinstein, J., 1989. Diffusion-controlled reactions. II. further bounds on the rate constant. J. Chem. Phys. 90, 1644–1647.

Torquato, S., Scardicchio, A., Zachary, C.E., 2008. Point processes in arbitrary dimension from fermionic gases, random matrix theory, and number theory. J. Stat. Mech. 2008, P11019.

Torquato, S., Stell, G., 1982. Microstructure of two-phase random media: I. the *n*-point probability functions. J. Chem. Phys. 77, 2071–2077.

Torquato, S., Stell, G., 1985. Microstructure of two-phase random media: V. the *n*-point matrix probability functions for impenetrable spheres. J. Chem. Phys. 82, 980–987.

Torquato, S., Stillinger, F.H., 2002. Controlling the short-range order and packing densities of many-particle systems. J. Phys. Chem. B 106, 8354–8359.

Torquato, S., Stillinger, F.H., 2003. Local density fluctuations, hyperuniform systems, and order metrics. Phys. Rev. E 68, 041113.

Torquato, S., Stillinger, F.H., 2006. New conjectural lower bounds on the optimal density of sphere packings. Exp. Math. 15, 307–331.

Torquato, S., Truskett, T.M., Debenedetti, P.G., 2000. Is random close packing of spheres well defined?,. Phys. Rev. Lett. 84, 2064–2067.

Torquato, S., Zhang, G., de Courcy-Ireland, M., 2019. Hidden multiscale order in the primes. J. Phys. A 52, 135002.

Torquato, S., Zhang, G., Stillinger, F.H., 2015. Ensemble theory for stealthy hyperuniform disordered ground states. Phys. Rev. X 5, 021020.

Uche, O.U., Stillinger, F.H., Torquato, S., 2004. Constraints on collective density variables: two dimensions. Phys. Rev. E 70, 46122.

Vasseur, J., Wadsworth, F.B., 2017. Sphere models for pore geometry and fluid permeability in heterogeneous magmas. Bull. Volcanol. 79, 77.

Weaire, D., Phelan, R., 1994. A counterexample to kelvin's conjecture on minimal surfaces. Phil. Mag. Lett. 69, 107–110.

Weijs, J.H., Jeanneret, R., Dreyfus, R., Bartolo, D., 2015. Emergent hyperuniformity in periodically driven emulsions. Phys. Rev. Lett. 115, 108301.

Weissberg, H.L., 1963. Effective diffusion coefficient in porous media. J. Appl. Phys. 34, 2636–2639.

Wood, B.D., Cherblanc, F., Quintard, M., Whitaker, S., 2003. Volume averaging for determining the effective dispersion tensor: closure using periodic unit cells and comparison with ensemble averaging. Water Resour. Res. 39, 1210. https://doi.org/10.1029/2002WR001723.

Yeong, C.L.Y., Torquato, S., 1998. Reconstructing random media. Phys. Rev. E 57, 495–506.

Yeong, C.L.Y., Torquato, S., 1998. Reconstructing random media: II. three-dimensional media from two-dimensional cuts. Phys. Rev. E 58, 224–233.

Zachary, C.E., Torquato, S., 2009. Hyperuniformity in point patterns and two-phase heterogeneous media. J. Stat. Mech. 2009, P12015.

Zachary, C.E., Torquato, S., 2011. Anomalous local coordination, density fluctuations, and void statistics in disordered hyperuniform many-particle ground states. Phys. Rev. E 83, 051133.

Zhang, G., Stillinger, F., Torquato, S., 2015. Ground states of stealthy hyperuniform potentials: I. Entropically favored configurations. Phys. Rev. E 92, 022119.

Zhang, G., Stillinger, F.H., Torquato, S., 2016. The perfect glass paradigm: disordered hyperuniform glasses down to absolute zero. Sci. Rep. 6, 36963.

Zhang, G., Stillinger, F.H., Torquato, S., 2016. Transport, geometrical and topological properties of stealthy disordered hyperuniform two-phase systems. J. Chem. Phys 145, 244109.

Zhang, G., Stillinger, F.H., Torquato, S., 2017. Can exotic disordered "stealthy" particle configurations tolerate arbitrarily large holes? Soft Matter 13, 6197–6207.

Zhou, W., Cheng, Z., Zhu, B., Sun, X., Tsang, H.K., 2016. Hyperuniform disordered network polarizers. IEEE J. Selected Topics in Quantum Elec. 22, 288–294.